Article

Compatibility rules of human enhancer and promoter sequences

https://doi.org/10.1038/s41586-022-04877-w

Received: 28 September 2021

Accepted: 17 May 2022

Published online: 20 May 2022

Check for updates

Drew T. Bergman[1,2,9], Thouis R. Jones[1,9], Vincent Liu[3], Judhajeet Ray[1], Evelyn Jagoda[1], Layla Siraj[1,4], Helen Y. Kang[3,5], Joseph Nasser[1], Michael Kane[1], Antonio Rios[3], Tung H. Nguyen[1], Sharon R. Grossman[1], Charles P. Fulco[1,8], Eric S. Lander[1,6,7] & Jesse M. Engreitz[1,3,5]✉

Gene regulation in the human genome is controlled by distal enhancers that activate specific nearby promoters[1]. A proposed model for this specificity is that promoters have sequence-encoded preferences for certain enhancers, for example, mediated by interacting sets of transcription factors or cofactors[2]. This 'biochemical compatibility' model has been supported by observations at individual human promoters and by genome-wide measurements in *Drosophila*[3–9]. However, the degree to which human enhancers and promoters are intrinsically compatible has not yet been systematically measured, and how their activities combine to control RNA expression remains unclear. Here we design a high-throughput reporter assay called enhancer × promoter self-transcribing active regulatory region sequencing (ExP STARR-seq) and applied it to examine the combinatorial compatibilities of 1,000 enhancer and 1,000 promoter sequences in human K562 cells. We identify simple rules for enhancer–promoter compatibility, whereby most enhancers activate all promoters by similar amounts, and intrinsic enhancer and promoter activities multiplicatively combine to determine RNA output ($R^2 = 0.82$). In addition, two classes of enhancers and promoters show subtle preferential effects. Promoters of housekeeping genes contain built-in activating motifs for factors such as GABPA and YY1, which decrease the responsiveness of promoters to distal enhancers. Promoters of variably expressed genes lack these motifs and show stronger responsiveness to enhancers. Together, this systematic assessment of enhancer–promoter compatibility suggests a multiplicative model tuned by enhancer and promoter class to control gene transcription in the human genome.

The extent to which distal enhancers might activate specific types of promoters has been an outstanding question in human gene regulation. Since their initial discovery, enhancers have been defined in part based on their ability to activate multiple non-cognate promoter sequences[10,11]. High-throughput reporter assays have now confirmed that many enhancer sequences derived from the human genome have the capability to activate various human, viral and synthetic promoters[12–18].

Yet, other observations have suggested that enhancers and promoters have some degree of intrinsic specificity. Early studies identified individual examples in which particular enhancers or cofactors showed stronger activation with certain core promoters[3–8]. More recently, studies using *Drosophila* and high-throughput reporter assays revealed that developmental and housekeeping gene promoters show greater than tenfold preferences for different classes of genomic enhancers[9], have differing levels of sequence-encoded responsiveness to enhancer activation[19] and respond differently to recruitment of various transcriptional cofactors[20]. Together, these studies have suggested a 'biochemical compatibility' model in which different enhancers might have an intrinsic preference for activating different promoter sequences based on the transcription factors (TFs) and cofactors that they can recruit[2,21].

Despite these advances, the biochemical compatibility model has not yet been systematically tested for human enhancers and promoters. As such, it remains unclear whether compatibility classes of enhancers and promoters exist in the human genome and, if so, how their enhancer and promoter activity combine and how such specificity is encoded.

Measuring enhancer–promoter compatibility

To investigate these questions, we developed an assay called ExP STARR-seq to test the ability of 1,000 candidate enhancers to activate 1,000 promoters (Fig. 1 and Extended Data Fig. 1). In this assay, we synthesized pools of enhancer and promoter sequences (264 bp) and

[1]Broad Institute of MIT and Harvard, Cambridge, MA, USA. [2]Geisel School of Medicine at Dartmouth, Hanover, NH, USA. [3]Department of Genetics, Stanford University School of Medicine, Stanford, CA, USA. [4]Biophysics Graduate Program, Harvard University, Cambridge, MA, USA. [5]BASE Initiative, Betty Irene Moore Children's Heart Center, Lucile Packard Children's Hospital, Stanford University School of Medicine, Stanford, CA, USA. [6]Department of Biology, MIT, Cambridge, MA, USA. [7]Department of Systems Biology, Harvard Medical School, Boston, MA, USA. [8]Present address: Bristol Myers Squibb, Cambridge, MA, USA. [9]These authors contributed equally: Drew T. Bergman, Thouis R. Jones. ✉e-mail: engreitz@stanford.edu

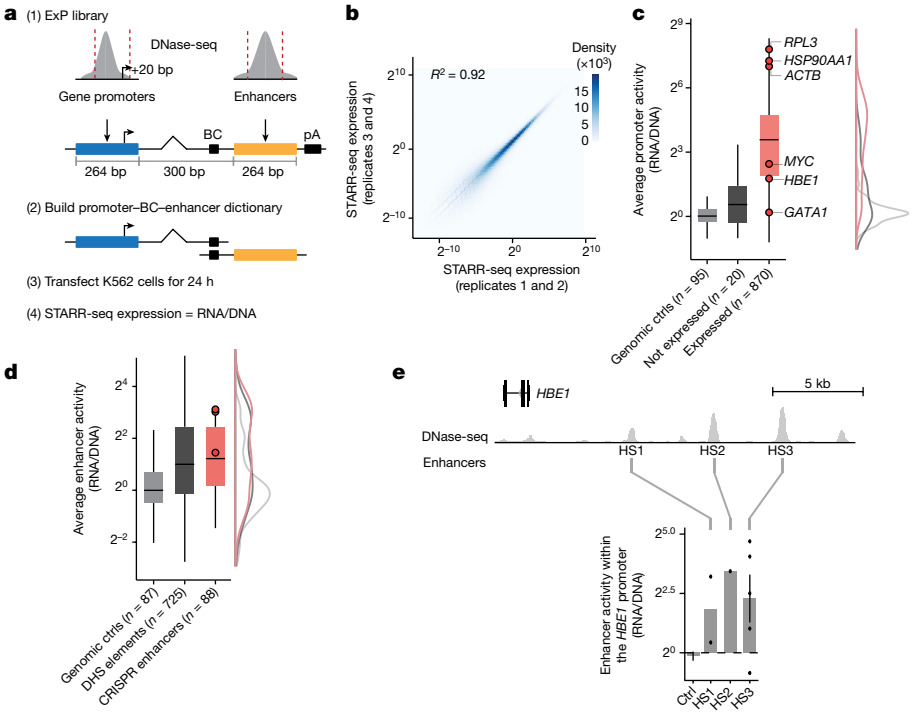

Fig. 1 | ExP STARR-seq. a, Schematic of the ExP STARR-seq method used to measure the activities of enhancer and promoter sequences and test their compatibilities. (1) Sequences 264 bp in length were selected and cloned in all pairwise combinations into the promoter and enhancer positions of a plasmid vector together with a plasmid barcode (BC). (2) We built a dictionary linking promoter–BC–enhancer triplets through sequencing (Extended Data Fig. 1a). (3) We then transfected the ExP STARR-seq plasmid pool into cells, in which the promoter sequence on a given plasmid initiates transcription of a polyadenylated RNA containing the plasmid BC and enhancer. (4) We sequenced these RNAs and calculated STARR-seq expression as the frequency of RNAs observed for each plasmid normalized by the frequency of that plasmid in the input DNA plasmid pool. **b**, Correlation of ExP STARR-seq expression between biological replicate experiments, calculated for individual enhancer–promoter pairs with unique plasmid BCs. Axes represent the average STARR-seq expression (RNA/DNA) of two biological replicates. Density indicates the number of enhancer–promoter plasmids. **c**, Average promoter activity (STARR-seq expression when paired with random genomic controls (ctrls) in the enhancer position) of promoter sequences derived from random genomic controls (set at 0), genes not expressed in K562s and all other gene promoters. Boxes represent the median and interquartile range (IQR), with whiskers ±1.5× the IQR. **d**, Average enhancer activity (STARR-seq expression of plasmids containing a given enhancer averaged across all promoters) of enhancer sequences derived from random genomic controls, accessible elements and genomic enhancers validated in CRISPR experiments. Boxes and whiskers as in **c**. Red dots represent three enhancers near *HBE1* (see **e**). **e**, Sequences derived from three genomic enhancers that regulate *HBE1* in the genome (HS1–HS3) activate the *HBE1* promoter in ExP STARR-seq. Ctrl, average of 44 random genomic control sequences in the enhancer position that passed thresholds (Methods). Error bars are 95% confidence intervals across plasmid BCs; $n = 110$ (Ctrl), 2 (HS1), 1 (HS2) or 5 (HS3).

cloned them in all pairwise combinations located about 340-bp apart in the modified human STARR-seq plasmid-based reporter vector[17] (Fig. 1a and Extended Data Fig. 1a). In STARR-seq assays, the enhancer sequence is transcribed and quantified using targeted RNA sequencing (RNA-seq) to determine the level of expression of each plasmid[13]. For ExP STARR-seq, we introduced a unique 16-bp plasmid barcode adjacent to the enhancer sequence that enabled us to determine which reporter transcripts are produced from which enhancer–promoter pair. We transiently transfected this pool of plasmids into cells, measured the level of reporter transcripts produced and calculated STARR-seq expression as the amount of RNA normalized to DNA input for each plasmid. This approach enabled us to quantitatively measure the expression of hundreds of thousands of combinations of enhancer and promoter sequences, estimate the activities of individual enhancers and promoters and test their compatibilities (Methods).

Hereafter, for clarity, we use the terms 'enhancer sequences' and 'promoter sequences' to refer to sequences cloned into the enhancer and promoter positions, respectively, in the ExP STARR-seq assay, and 'genomic enhancers' and 'genomic promoters' to refer to the corresponding elements in the genome.

ExP STARR-seq was used to examine the combinatorial activities of 1,000 enhancer and 1,000 promoter sequences (Supplementary Tables 1 and 2) in K562 erythroleukaemia cells, which have been deeply profiled by the ENCODE Project[1] and for which we have previously collected data about which genomic enhancers regulate which genomic promoters using CRISPR interference (CRISPRi) screens[22]. Here we selected the following promoter sequences for inclusion: (1) 65 genes studied in prior CRISPR screens; (2) 735 additional genes sampled from across the genome to span a range of transcriptional activity (based on precision run-on sequencing (PRO-seq) data in K562 cells); and (3) 200 control sequences, including random genomic control sequences that are not accessible by assay for transposase-accessible chromatin using sequencing (ATAC-seq), and dinucleotide shuffled sequences (Extended Data Fig. 1a and Methods). The promoter sequences were chosen to include approximately 20 bp downstream of the genomic transcription start site (TSS) (as observed in capped analysis of gene expression (CAGE) data) and approximately 242 bp upstream (264 bp in total; Methods). In the enhancer position of ExP STARR-seq, we included the following elements: (1) 131 accessible genomic elements we previously tested by CRISPRi; (2) 669 other accessible genomic elements selected to span a range of quantitative histone 3 lysine 27 acetylation (H3K27ac) and DNase-based sequencing (DNase-seq) signals (centred on the summit of the DNase-seq peak); and (3) 200 controls, including random genomic control sequences and dinucleotide shuffled sequences (Extended Data Fig. 1a and Methods).

We cloned these 1,000 enhancer and 1,000 promoter sequences in all pairwise combinations, transfected the plasmid pool into K562 cells in 4 biological replicates of 50 million cells each and sequenced each STARR-seq RNA and input DNA library to a depth of at least 2.6 billion and 470 million reads, respectively (Extended Data Fig. 1c). We focused our analysis on the 604,268 enhancer–promoter pairs for which we obtained good coverage (Methods). STARR-seq expression (RNA/DNA) varied over six orders of magnitude and was highly reproducible when comparing the following expression values: individual plasmid barcodes between biological replicates (R^2 = 0.92; Fig. 1b and Extended Data Fig. 1b); an enhancer–promoter pair averaged across plasmid barcodes between biological replicates (R^2 = 0.92); and different plasmid barcodes for a given enhancer–promoter pair (R^2 = 0.62; Extended Data Fig. 1d–f and Methods).

Promoter sequences showed a large (>1,500-fold) dynamic range of expression levels, similar to previous studies[23] (average promoter activity = STARR-seq expression averaged across pairings with the 200 random genomic control sequences in the enhancer position). The strongest promoters in the dataset corresponded to housekeeping genes such as *RPL3*, *HSP90AA1* and *ACTB*, whereas the weakest promoters included shuffled control sequences and non-expressed genes in K562 cells (Fig. 1c). Enhancer sequences also showed a wide (682-fold) range of STARR-seq expression in the dataset when averaged across promoters (average enhancer activity), and were on average twofold more active than random genomic control sequences (Fig. 1d and Extended Data Fig. 1i). Enhancer and promoter activity from ExP STARR-seq results correlated with biochemical features of activity at the corresponding genomic elements, including levels of chromatin accessibility, H3K27ac level and nascent gene and enhancer RNA transcription (Extended Data Fig. 1g).

Sequences derived from known genomic enhancers also activated their cognate promoters in the ExP STARR-seq assay. For example, we included three enhancers in the β-like globin locus control region (HS1–HS3) that coordinate expression of haemoglobin subunits during erythrocyte development[24,25] and for which CRISPRi perturbations in K562 cells reduce the expression of haemoglobin subunit epsilon 1 (*HBE1*) by 10–86% (refs. [26,27]). In ExP STARR-seq, each of these enhancers activated the *HBE1* promoter (by 5.21-fold to 15.9-fold versus random genomic controls; Fig. 1e). Similarly, an enhancer that we previously showed to regulate *GATA1* and *HDAC6* in the genome[28] led to 6.76-fold and 6.87-fold activation of the *GATA1* and *HDAC6* promoters, respectively, in ExP STARR-seq (Extended Data Fig. 1h).

Taken together, these results show that ExP STARR-seq produces quantitative and reproducible measurements of enhancer and promoter sequence activity over a large dynamic range.

Broad enhancer–promoter compatibility

We used this ExP STARR-seq dataset to test whether specific enhancers activate specific promoters. Notably, nearly all active enhancer sequences activated all promoter sequences by similar amounts. For example, a small subset of five enhancers activated five promoters by a similar fold-change, even though the promoters spanned a 5.62-fold range of basal activities (Extended Data Fig. 2a,b; each enhancer–promoter pair had good coverage in the assay, median = 27 plasmid barcodes per pair). More generally, enhancers activated most promoters by similar fold-changes, with an average Spearman correlation of 0.81 across all pairs of promoters (Fig. 2a,c and Extended Data Fig. 2c). Moreover, pairs of enhancers showed similar proportional activation of promoters, with an average Spearman correlation of 0.72 (Fig. 2b,d and Extended Data Fig. 2d,e). These observations indicate that in this STARR-seq assay, there is broad compatibility between individual enhancer and promoter sequences, which is a marked difference from previous observations in *Drosophila*[9,19].

Activities multiplicatively combine

This pattern of effects—in which enhancers showed similar fold-activation across many promoters, and promoters showed similar levels of activation by many enhancers—suggests that intrinsic enhancer and promoter activities multiplicatively combine to produce the RNA output in STARR-seq. To quantify this, we correlated expression in the STARR-seq assay with intrinsic enhancer activity, intrinsic promoter activity and the multiplicative product of intrinsic enhancer and promoter activities.

To do so, we fit the following Poisson count model:

$$\mathrm{RNA} \sim \mathrm{Poisson}(k \times \mathrm{DNA} \times P \times E),$$

where RNA is RNA reads counts per plasmid, DNA is DNA read counts per plasmid, P is the intrinsic promoter activity, E is intrinsic enhancer activity and k is a free intercept term used to scale the activities of promoters, enhancers and their pairings relative to the average of random genomic control sequences (Methods). This multiplicative model assumes that there is no sequence or biochemical specificity between individual pairs of enhancers and promoters, and that differences in expression are solely due to differences in intrinsic enhancer and promoter activities. Hereafter, we define 'intrinsic enhancer activity' and 'intrinsic promoter activity' as the fits from this model, which are similar to the 'average activities' calculated above (Extended Data Fig. 2f,g) but better account for missing data and counting noise (Methods). These estimates of activity were reproducible across replicate experiments and when comparing non-overlapping plasmid barcodes (Extended Data Fig. 2h,i).

The multiplicative combination of intrinsic promoter and enhancer activities explained 82% of the total variance in STARR-seq expression, whereas intrinsic promoter and enhancer activities alone explained 48% and 27%, respectively (correlation with $\log_2$(STARR-seq expression) across all enhancer–promoter pairs with at least 2 plasmid barcodes; Fig. 2e–i). The multiplicative model fit similarly well between enhancer–promoter pairs located near to one another in the genome (<10 kb and <100 kb), as it did for enhancer–promoter pairs located on different chromosomes (Extended Data Fig. 2j). From the point of view of enhancer activation (fold-activation of an enhancer on a promoter, normalizing out promoter strength), intrinsic enhancer activity explained 65% of the variance, with 35% unexplained (Extended Data Fig. 2k). At least part of the remaining variance is probably due to experimental noise, because the proportion of variance explained by the multiplicative model increased when we examined *E*–*P* pairs with ≥20 barcodes (increasing from 82% to 94% variance explained for STARR-seq expression, and from 65% to 89% explained by intrinsic enhancer activity for enhancer activation) (Extended Data Fig. 2l).

To confirm that this multiplicative relationship is not due to the specific design of our ExP STARR-seq assay, we cloned 7 enhancers from the *MYC* locus (1.0–2.2 kb) and 5 promoter sequences (138–908 bp, including the promoters of *MYC* and other nearby genes) in all combinations into a different reporter plasmid in which the enhancer is located 1 kb upstream of the promoter, and measured the expression of these constructs using a luciferase reporter assay (Extended Data Fig. 3a and Supplementary Table 3). Despite a range of intrinsic promoter activities (Extended Data Fig. 3b), all enhancer sequences activated all promoter sequences by a similar fold-change, and a multiplicative function of enhancer and promoter activities explained 84% of the total variance in the measurements (Extended Data Fig. 3c). We further tested whether gene transcription in the genome (as measured by PRO-seq) could be modelled as a multiplicative function of promoter activity (measured by STARR-seq) and enhancer inputs. Here this was calculated as the sum of activity-by-contact (ABC) scores[22] for all nearby enhancers, which allowed us to include all enhancers in each locus, including those not tested in ExP STARR-seq. Gene transcription correlated with this

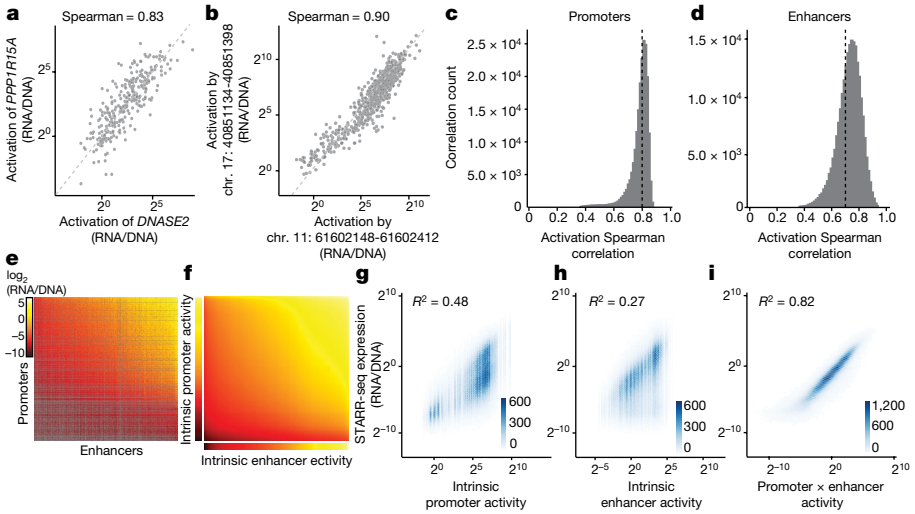

Fig. 2 | Enhancer and promoter activities combine multiplicatively. **a**, Correlation of enhancer activation for *PPP1R15A* and *DNASE2* promoters. Each point is a shared enhancer sequence. **b**, Correlation of enhancer activation by chr. 17: 40851134-40851398 and chr. 11:61602148–61602412 enhancers. Each point is a shared promoter sequence. **c**, Distribution of pairwise correlations of enhancer activation between promoter sequences (as in **a**). The black dotted line indicates the mean Spearman correlation. **d**, Distribution of pairwise correlations of promoter activation between enhancer sequences (as in **b**). The black dotted line indicates the mean Spearman correlation. **e**, Heatmap of ExP STARR-seq expression across all pairs of promoter (vertical) and enhancer sequences (horizontal). Axes are sorted by intrinsic promoter and enhancer activities. Grey indicates missing data. **f**, Heatmap representing the multiplication of intrinsic promoter activity (vertical) with intrinsic enhancer activity (horizontal) from the Poisson model. **g**–**i**, Correlation of ExP STARR-seq expression with intrinsic promoter activity (**g**), intrinsic enhancer activity (**h**) and the product of intrinsic promoter and enhancer activities (**i**). The density colour scale indicates the number of enhancer–promoter pairs.

promoter activity × enhancer input model ($R^2 = 0.378$) much better than with either promoter activity or enhancer inputs alone ($R^2 = 0.128$ and 0.245, respectively) (Extended Data Fig. 3d–f).

Thus, RNA expression in these reporter assays represents, to a first approximation, the multiplicative product of intrinsic enhancer activity and intrinsic promoter activity.

Classes of enhancers and promoters

Although we did not observe a strong degree of specificity among enhancer and promoter sequences, we asked whether there might be classes with more subtle, quantitative preferences. To do so, we calculated for each enhancer–promoter pair its deviation from the multiplicative enhancer × promoter model (observed STARR-seq expression versus the product of intrinsic enhancer activity and intrinsic promoter activity; Methods).

We identified two clusters of enhancer sequences (E1 and E2, $n = 126$ and 290, respectively) that showed differential effects with respect to two sets of promoter sequences (P1 and P2, $n = 192$ and 391 respectively) (Fig. 3a and Extended Data Fig. 4). In particular, E1 enhancer sequences activated P1 promoters more strongly than P2 promoters (by 1.93-fold, $P = 4.19 \times 10^{-8}$, *t*-test), whereas E2 enhancer sequences activated promoters in both clusters to an approximately equal degree (1.05-fold stronger for P2 versus P1, $P = 0.424$, Student's *t*-test; Fig. 3b). These sets of enhancers and promoters appeared to represent extremes of a graded scale, whereby promoter responsiveness to E1 versus E2 enhancer sequences varied over about a threefold range (Fig. 3c and Extended Data Figs. 4d,g and 5a), and enhancer activation of P1 versus P2 promoters varied over about a twofold range (Fig. 3d and Extended Data Figs. 4e,h and 5b). Cluster assignments were stable to downsampling of promoter and enhancer sequences (Extended Data Fig. 4f and Methods). Two additional clusters, P0 and E0, contained the remaining sequences, which had extremely weak activity and/or missing data and are excluded from analysis in subsequent sections (Extended Data Fig. 4a–c).

We quantified the additional variance explained by promoter and enhancer class by extending the multiplicative ExP model as follows:

$$\mathrm{RNA} \sim \mathrm{Poisson}(k \times \mathrm{DNA} \times P \times E \times \mathrm{PEClassInteraction}),$$

where PEClassInteraction is a weighted indicator variable for each of the nine possible *E*–*P* class combinations. Promoter and enhancer class specificity explained an additional 2% of the total variation in STARR-seq expression or, after normalizing for promoter activity, an additional 4% of the variance in enhancer activation (Extended Data Fig. 2k).

Together, these observations identify classes of enhancer and promoter sequences with subtle quantitative differences in compatibility. We next sought to characterize these classes to understand how such preferential effects might be encoded.

Properties of enhancer classes

To characterize the two classes of ExP STARR-seq enhancer sequences, we compared the classes with respect to biochemical features of their corresponding elements in the genome, sequence motifs, effects in CRISPR experiments and other features.

E1 and E2 classes showed biochemical features of strong and weak genomic enhancers, respectively. The features most strongly associated with E1 compared with E2 sequences in the genome included H3K27ac, DNase I hypersensitivity, AP-1 factor binding (JUN and ATF3) and other known activating TFs (Fig. 3a, Extended Data Fig. 6a–d and Supplementary Table 4). E2 sequences in the genome were also DNase accessible and sometimes bound these factors, but to a significantly lesser degree. Consistent with these observations, E1 sequences had stronger effects on gene expression in CRISPR perturbation experiments, even when controlling for 3D contact with the target gene (Extended Data Fig. 6e). E1 sequences were more likely to be predicted to be enhancers in K562 cells (94% of E1 predicted to regulate a gene by the ABC model versus 49% of E2), and more likely to be broadly active in many cell types (32% of E1 predicted to be ABC enhancers in >50 of 130 other biosamples,

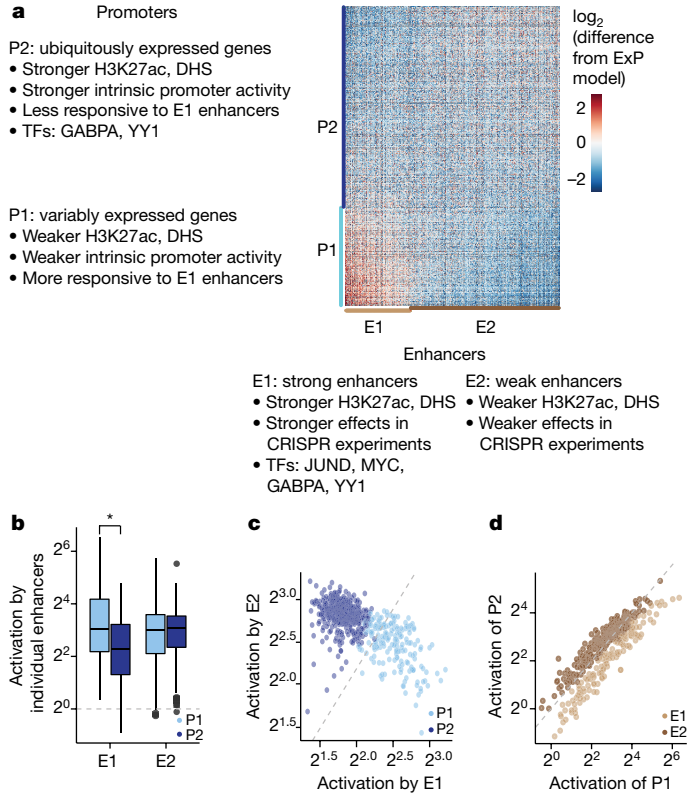

Fig. 3 | Compatibility classes of enhancers and promoters. a, Heatmap of deviations in enhancer–promoter STARR-seq expression from a multiplicative enhancer–promoter model (colour scale indicates the fold-difference between observed expression versus expression predicted by the multiplicative model; grey indicates missing data). The vertical axis shows promoter sequences grouped by class and sorted by responsiveness to E1 versus E2 (see **b**); the horizontal axis shows enhancer sequences grouped by class and sorted by activation of P1 versus P2 (see **c**). **b**, Activation of P1 versus P2 promoters by E1 and E2 enhancer sequences (equivalently: responsiveness to E1 versus E2 enhancer sequences). $n = 126$ (E1) or 290 (E2). Boxes represent the median and IQR, with whiskers ±1.5× the IQR. $^{*}P = 4.2 \times 10^{-8}$, two-sample *t*-test. **c**, For each promoter, the average activation by (responsiveness to) E1 enhancer sequences (*x* axis) versus the average activation by E2 enhancer sequences (*y* axis). P1 promoters are activated more strongly by E1 versus E2 enhancers. **d**, For each enhancer, the average fold-activation when paired with P1 promoters (*x* axis) versus P2 promoters (*y* axis). E1 enhancers more strongly activate P1 promoters.

versus 13% of E2; Extended Data Fig. 6f). Both classes contained a large fraction of sequences predicted to be an enhancer in at least one other related or unrelated cell type (90% of E1 and 70% of E2), which suggests that some E2 genomic elements may act as strong enhancers in other cell types. Regarding sequence features, E1 enhancer sequences were significantly enriched for FOS and JUN motifs, whereas E2 enhancer sequences were not significantly enriched for any particular motif (Benjamini–Hochberg corrected $P < 0.05$; Extended Data Fig. 6b,c and Supplementary Table 5). Both E1 and E2 genomic enhancers appeared to produce enhancer RNAs, as measured by global nuclear run-on sequencing (GRO-cap) (Extended Data Fig. 6g), and showed similar levels of sequence conservation (Extended Data Fig. 6h).

These observations suggest that the differences in how these classes of enhancer sequences activate different promoters in ExP-STARR-seq could be related to their ability to recruit activating TFs (see below). We note that despite these clear differences in genomic activity, the two classes of enhancer sequences showed, on average, similar levels of activity in the ExP-STARR-seq assay (Extended Data Fig. 4b). This may reflect previous observations that sequences in STARR-seq might affect reporter expression by acting on steps other than transcriptional activation[16] or that the episomal STARR-seq assay often detects activity for sequences that do not appear to be active in their endogenous chromosomal context[17,29].

Properties of promoter classes

The two classes of promoter sequences also showed marked differences in their functional annotations, intrinsic promoter activity and responsiveness to enhancers in the genome.

Many P2 promoter sequences corresponded to ubiquitously and uniformly expressed genes (often referred to as housekeeping genes), whereas P1 promoters largely corresponded to genes that were more variably expressed across cell types (Fig. 4a). For example, P2 promoters included β-actin (*ACTB*), all 37 tested ribosomal subunits (for example, *RPL13* and *RPS11*), components of the electron transport chain (for example, *NDUFA2* and *ATP5B*), among others (Supplementary Table 1). By contrast, P1 promoters included erythroid-specific genes (for example, three haemoglobin genes) and variably expressed TFs (for example, *KLF1*, *JUNB*, *REL* and *MYC*). Across a panel of 131 cell types and tissues (biosamples), most P2 promoters (76%) were active in all 131 biosamples compared with only 45% of P1 promoters (Extended Data Fig. 7a). Moreover, P1 and P2 promoters were associated with 'developmental' and 'housekeeping' gene ontology terms, respectively (Extended Data Fig. 7b).

P1 promoters had on average 3.2-fold weaker intrinsic promoter activity than P2 promoters, as measured by ExP STARR-seq ($P < 10^{-16}$, Mann–Whitney *U*-test; Fig. 4b and Extended Data Fig. 4b), but showed similar levels of transcription in their native genomic locations (as measured by PRO-seq in the gene body; $P = 0.733$, Mann–Whitney *U*-test; Fig. 4b). P1 promoters also had more activating chromatin environments based on predictions of enhancer input from the ABC model ($P = 0.00083$, Mann–Whitney *U*-test; Extended Data Fig. 7c–e). This suggests that P1 promoters may be more dependent on the genomic context for their level of transcription in the genome.

Indeed, genes corresponding to P1 promoters had more genomic regulatory elements in CRISPR experiments. In data from previous studies in which CRISPRi was used to perturb every DNase-accessible element near selected promoters (Methods), the 14 genes corresponding to P1 promoters had an average of 3.6 (median of 3) distal enhancers in CRISPR experiments, whereas the 11 genes corresponding to P2 promoters had only 0.36 (median of 0; Fig. 4c and Extended Data Fig. 7f). Distal enhancers for P1 genes in the genome also had stronger effect sizes ($P = 0.0071$, *t*-test, Extended Data Fig. 7g).

Together, these observations suggest that P1 promoter sequences correspond to variably expressed genes and depend more on distal enhancers for their transcriptional activation both in the ExP STARR-seq assay and in the genome, whereas P2 promoter sequences correspond to ubiquitously expressed genes that are relatively less sensitive to distal enhancers in both contexts.

TFs distinguish promoter classes

We next sought to identify sequence and chromatin features that distinguish P1 (more responsive) from P2 (less responsive) promoters.

We considered canonical core promoter motifs, which have been observed to differ between various subsets of promoters[30–34], but did not find strong relationships. P1 and P2 promoter sequences had similar frequencies of the canonical 'CA' initiator dinucleotide at the TSS (40.1% versus 35.3%; Extended Data Fig. 7h), and corresponded to genes with similar patterns of dispersed versus focused TSSs in the genome (Extended Data Fig. 7i). Consistent with previous studies[30–34] comparing features of housekeeping versus other gene promoters, P2 promoters had a slightly higher frequency of CpG dinucleotides (median of 0.90 versus 0.81 normalized CpG content

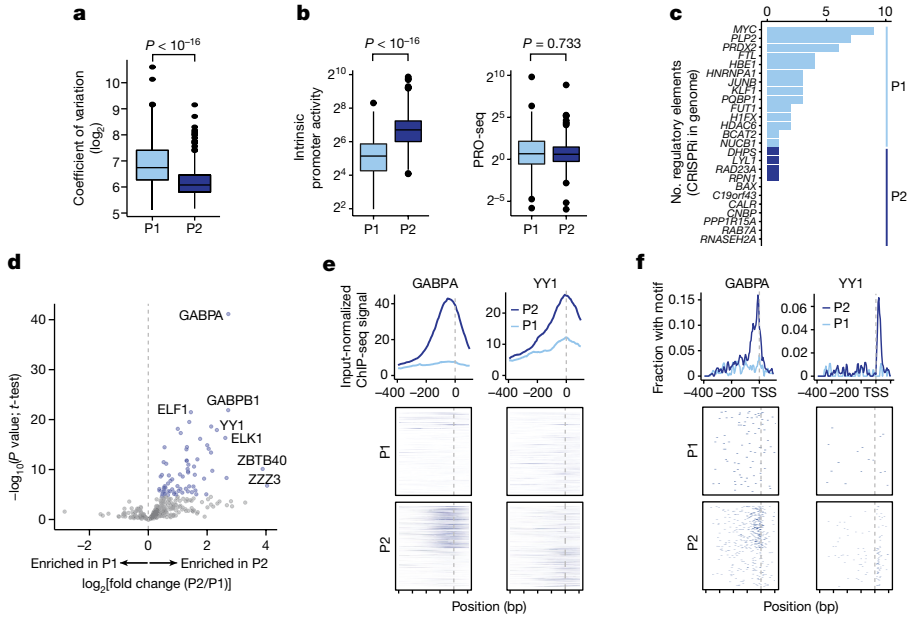

Fig. 4 | Promoter classes correspond to enhancer responsive versus ubiquitously expressed genes. a, Variability of expression of genes across cell types corresponding to P1 and P2 promoters. Coefficient of variation is calculated across 1,829 CAGE experiments from the FANTOM5 Consortium[48]. $n = 192$ (P1) or 391 (P2). P value is from two-sample t-test. **b**, Left, Intrinsic promoter activity for P1 versus P2 promoters (ExP STARR-seq). Right, Genomic transcription level of genes corresponding to P1 versus P2 promoters (PRO-seq reads per kilobase per million in gene bodies). $n = 192$ (P1) or 391 (P2). P value is from two-sample t-test. **c**, Number of activating genomic regulatory elements identified in comprehensive CRISPRi screens for genes corresponding to P1 promoters ($n = 14$) and P2 promoters ($n = 11$)[22]. **d**, Volcano plot comparing ChIP-seq and other biochemical features for P2 versus P1 promoters (Supplementary Table 6). x axis shows the ratio of average signal at P2 versus P1 promoters. Blue points indicate features with significantly higher signals at P2 promoters; no features have significantly higher signals at P1 promoters. **e**, ChIP-seq signal for GABPA and YY1 in K562 cells at P1 and P2 promoters in the genome aligned by the TSS (Methods). Top, average ChIP signal (normalized to input) ±95% confidence intervals. Bottom, Signals at individual genomic promoters. **f**, Motif occurrences for GABPA and YY1 in P1 and P2 promoters aligned by the TSS. For **a** and **b**, boxes represent the median and IQR, with whiskers ±1.5× the IQR.

for P2 and P1 promoters; Extended Data Fig. 7j), and P1 promoters had a twofold higher frequency of TATA box sequences upstream of the TSS (12.5% versus 6.1%), although only a small proportion of promoters contained this motif (Extended Data Fig. 7h). Both groups of promoters showed similar levels of sequence conservation (Extended Data Fig. 7k).

Accordingly, we explored which other sequence features or TF binding measurements distinguished P2 from P1 promoters. We examined 3,206 other features (including measurements from chromatin immunoprecipitation with sequencing (ChIP-seq) assays, TF motif predictions and other features) and identified marked differences in the frequencies of certain TF binding sites and motifs (Fig. 4d, Extended Data Fig. 7l–m and Supplementary Tables 6 and 7). In combination, these features could classify the two promoter classes with 94% accuracy in 6-fold cross-validation (Supplementary Table 8 and Methods). The most significantly enriched features included a ChIP-seq signal for ETS family factors (GABPA, ELK1, ELF1), YY1, HCFC1, NR2C1 and C11orf30 (also known as EMSY) (Fig. 4d and Extended Data Fig. 8a). For example, two of the top factors (GABPA and YY1) together showed strong binding to a total of 64% of P2 promoters in the genome. That is, 50% of P2 promoters showed strong GABPA binding (versus 8% of P1 promoters; $P = 9.9 \times 10^{-22}$, Benjamini–Hochberg-corrected Fisher's exact test), and 29% of P2 promoters showed strong YY1 binding (versus 5% of P1 promoters; $P = 9.4 \times 10^{-9}$, Benjamini–Hochberg-corrected Fisher's exact test) (Fig. 4e). Notably, the sequence motifs for these factors showed positional preferences consistent with a function in regulating transcription initiation. The motif for GABPA was typically located 0–20 nucleotides upstream of the TSS (mode of −10), and for YY1, the motif was often positioned at either +18 bp (both strands) or +2 bp (negative strand) from the TSS (Fig. 4f, Extended Data Fig. 7n). Consistent with these factors having a functional role, previous studies have found that adding GABPA or YY1 motifs to promoters increases gene expression in various reporter assays and cell types[35–38].

Together, these analyses suggest that P2 promoters can best be distinguished from P1 promoters by the presence of certain TFs, including GABPA and YY1, rather than canonical core promoter motifs.

P2 promoters contain built-in enhancers

We considered how TFs such as GABPA and YY1 might contribute to the reduced enhancer responsiveness of P2 versus P1 promoters. Notably, these same factors showed strong binding in the genome not only at P2 promoters (Fig. 4e,f) but also at some E1 enhancers (Extended Data Figs. 6a and 8b). For example, three of the genomic enhancers for *HBE1* (all classified as E1 in ExP STARR-seq) contained GABPA sequence motifs and showed strong GABPA binding by ChIP-seq, whereas the genomic promoter of *HBE1* (classified as P1) lacked these features (Fig. 5a).

These observations suggest that P2 promoters may have reduced responsiveness to E1 enhancers because they contain some of the same motifs, which potentially saturate a particular step in transcription. Accordingly, we explored the hypothesis that promoters contain built-in E1 enhancer sequences that would increase promoter activity and decrease responsiveness to distal E1 enhancers.

Consistent with this hypothesis, the following results were obtained. (1) Across all promoters, responsiveness to E1 enhancers was inversely correlated with intrinsic promoter activity in a way that appeared to reach saturation. (2) P2 promoters had stronger enhancer activity than P1 promoters. (3) Nearly all of the TF motifs enriched in P2 promoters were predictive of both promoter activity and enhancer activity. And (4) scrambling or inserting GABPA or YY1 motifs affected the responsiveness of promoters to E1 enhancers.

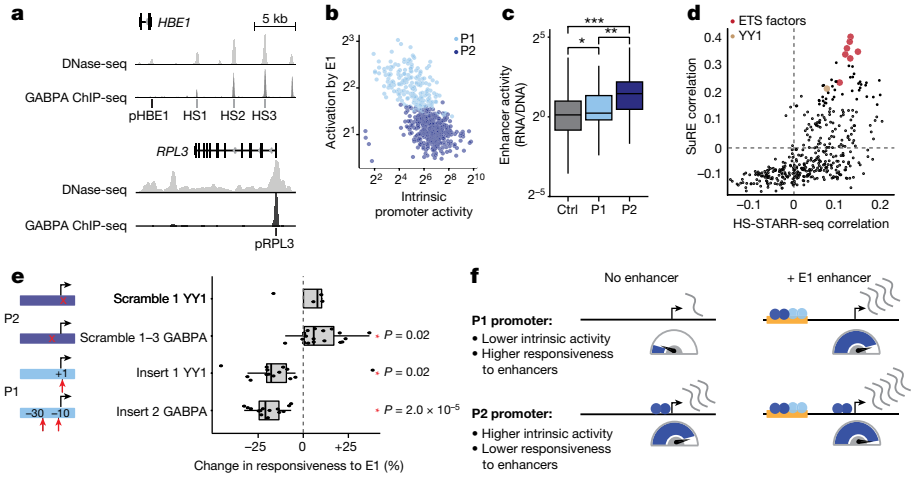

Fig. 5 | P2 promoters contain built-in enhancer sequences. a, DNase-seq and GABPA ChIP-seq binding at the *HBE1* promoter (pHBE1, P1), HS1–HS3 enhancers (E1) and *RPL3* promoter (pRPL3, P2). **b**, Correlation between intrinsic promoter activity and responsiveness of promoters to E1 enhancers (average activation by E1 sequences, expressions versus random genomic controls). Each point is one promoter. **c**, Average enhancer activity in HS-STARR-seq (RNA/DNA) of random genomic background fragments (Ctrl, $n = 3.9$ million) and P1 ($n = 192$) and P2 ($n = 391$) promoters. $^{*}P = 5.2 \times 10^{-4}$, $^{**}P = 1.1 \times 10^{-15}$, $^{***}P = 1.4 \times 10^{-66}$, two-sided *t*-test. **d**, For each of the 400 sequence motifs that appeared in at least 5% of HS-STARR-seq fragments, shown are correlations (Pearson *R*) of motif occurrence with intrinsic promoter activity (SuRE signal, *y* axis) with intrinsic enhancer activity (HS-STARR-seq signal among fragments not overlapping TSS, *x* axis). **e**, Change in promoter responsiveness to E1 enhancers (average fold-activation by E1 enhancers) after scrambling YY1 or GABPA motifs in P2 promoters or inserting YY1 or GABPA motifs into P1 promoters. Each point is a promoter. $^{*}P < 0.05$, two-sided *t*-test. **f**, A model for enhancer–promoter compatibility. Enhancers multiplicatively scale the RNA output of promoters. P2 promoters contain built-in activating sequence motifs that both increase intrinsic promoter activity and reduce the responsiveness to distal enhancers. For **c** and **e**, boxes represent the median and IQR, with whiskers ±1.5× the IQR.

We first compared intrinsic promoter activity with responsiveness to E1 enhancers. These two factors were correlated both when considering all promoters in ExP STARR-seq (Pearson $R = -0.62$, $\log_2$(space); Fig. 5b) and when considering only P1 promoters ($R = -0.51$). As promoter activity increased, responsiveness to E1 enhancers rapidly decreased (for example, from about ninefold average activation by E1 enhancers for the *SNAI3* P1 promoter) and appeared to saturate at about threefold for most P2 promoter sequences (Extended Data Fig. 8c).

We next tested whether P2 promoters had stronger intrinsic enhancer activity. To do so, we generated a second STARR-seq dataset in which we measured the enhancer activity of >8.9 million sequences derived from DNase-accessible elements and promoters (by hybrid selection (HS) STARR-seq; Methods and Extended Data Fig. 8d–f). In this dataset, many promoter elements tested in ExP STARR-seq (along with thousands of other accessible elements) were densely tiled (an average of about 11 fragments each covering at least 90% of the promoters tested in the ExP assay), which enabled us to test the enhancer activity of entire P1 and P2 promoter sequences. P2 promoters indeed showed about twofold higher intrinsic enhancer activity than P1 promoters in HS-STARR-seq ($P = 1.14 \times 10^{-16}$, *t*-test; Fig. 5c), which provides support for a model in which these promoters contain built-in enhancers.

We examined whether the sequence motifs enriched in P2 promoters contribute to both enhancer activity and promoter activity. To do so, we examined data on enhancer activity from HS-STARR-seq along with another previous experiment that measured promoter activity for millions of random genomic fragments in K562 cells (survey of regulatory elements (SuRE)[23]). A total of 16 out of the 17 motifs enriched in P2 promoters, including motifs for GABPA and YY1, were positively correlated with both enhancer activity and promoter activity (Fig. 5d, Supplementary Table 9 and Methods).

Finally, we conducted an ExP STARR-seq experiment in which we scrambled or inserted TF motifs into promoter or enhancer sequences (Fig. 5e and Extended Data Fig. 9a–d). As predicted, inserting GABPA or YY1 motifs into P1 promoter sequences significantly decreased the responsiveness to E1 enhancers (GAPBA: average of −19.8%, $P = 2.0 \times 10^{-5}$; YY1: average of −14.8%%, $P = 0.02$; $n = 14$ insertions each). Conversely, mutating one or more motifs in P2 promoter sequences usually increased the responsiveness to E1 enhancers (GABPA: average of +8.9%, $P = 0.02$, $n = 20$; YY1: average of +2.6%, $P = 0.7$, $n = 4$). We also tested the effect of inserting GABPA motifs into E0 (very weak) enhancer sequences. Such motifs increased enhancer activity, more so for P1 compared with P2 promoters (average of +1,289% with P1, average of +417% with P2, $P = 7.9 \times 10^{-14}$; Extended Data Fig. 9d).

Together, these observations suggest a model for promoter sequence organization (Fig. 5f). Promoters encode binding motifs for activating factors, including GABPA and YY1, that act as built-in enhancers for the promoter. This not only increases the autonomous activity of the promoter but also reduces its responsiveness to distal enhancers. Although P2 promoters have strong built-in enhancers, P1 promoters appear to have weaker or fewer built-in activating motifs, which renders them more sensitive to distal enhancers.

Compatibility rules in a second dataset

A parallel study[39] conducted a similar experiment to examine the compatibilities among hundreds of enhancer and promoter sequences in mouse embryonic stem cells (a total of 22,406 enhancer–promoter pairs, measured in 2 separate experiments). This dataset provided an opportunity to assess the extent to which the compatibility rules we identified generalize to a second cell type, organism and assay format. Regarding the assay format, that study[39] used a different plasmid design (massively parallel reporter assay (MPRA) format with the enhancer located immediately upstream of the promoter), different method of element selection (densely sampled from 3 genomic loci) and different enhancer and promoter sequence lengths (about 400 bp).

The patterns of enhancer–promoter compatibility in this second dataset were highly similar to ExP STARR-seq. The multiplicative enhancer × promoter model explained 91% and 78% of the variance in RNA expression in the two experiments and 81% and 34% of the variance in enhancer activation (Extended Data Fig. 9e,f). The fraction of variance unexplained could result in part from additional specificity factors (see also ref. [39]). Promoters with stronger intrinsic activity were less

sensitive to activation by enhancer sequences, and ETS-family motifs, including GABPA, were the strongest motifs that were positively correlated with enhancer activity and negatively correlated with enhancer responsiveness (see also ref. [39]), which is consistent with features of P1 and P2 promoters identified in ExP STARR-seq. We note that the previous analysis[39] showed that most enhancers in both their MPRA and our ExP STARR-seq experiments showed significant deviations from the multiplicative model, but the magnitude of such deviations is small and explain only a small fraction of the variance in reporter expression (Extended Data Fig. 9e,f). Together, both datasets indicate that across multiple cell types and mammalian genomes, enhancers and promoters are broadly compatible and there is an additional layer of selectivity in which specific motifs, such as for GABPA and YY1, can tune enhancer–promoter activation.

Discussion

Since the discovery of the first enhancers 40 years ago[10,11], many enhancer and promoter sequences have been combined and found to be compatible[12–18]. At the same time, studies of individual natural or synthetic core promoters have been found to have some degree of specificity when combined with various transcriptional cofactors or enhancer sequences[3–8].

Here we developed and applied ExP STARR-seq to systematically quantify enhancer–promoter compatibility and identified a simple rule for combining human enhancer and promoter activities. Enhancers are intrinsically compatible with many RNA polymerase II promoter sequences and act multiplicatively to scale the RNA output of a promoter. As a result, independent control of intrinsic enhancer activity and intrinsic promoter activity can create significant variation in RNA expression. In our data, promoter activity and enhancer activity each vary by more than three orders of magnitude, with their multiplicative combination explaining much of the observed >250,000-fold variation in STARR-seq expression (Fig. 2i and Extended Data Fig. 2k–l). This broad compatibility appears to be consistent with recent studies that used other reporter approaches. That is, human core promoters or enhancers are similarly scaled when they are inserted into different genomic loci[40,41], and randomly generated enhancer and promoter sequences combine multiplicatively in STARR-seq experiments in three other cell lines[36]. This is also consistent with our previous finding[22] that the effects of enhancers on nearby genes in the genome can be predicted with good accuracy using the ABC model. This model assumes that all enhancers and promoters are equally compatible and that enhancer activity and 3D enhancer–promoter contact frequencies tune the relative effect of an enhancer on gene expression.

We also identified two classes of enhancers and promoters that have subtle preferences in activation. One class of promoters, corresponding largely to ubiquitously expressed (housekeeping) genes, is less responsive to distal enhancers both in ExP STARR-seq and in the genome, whereas the second class of promoters, corresponding to variably expressed genes, is more responsive. Previous studies have identified numerous differences in sequence content and motifs between the promoters of housekeeping and context-specific genes[30–34]. We found that these promoters indeed showed intrinsic differences in their levels of activity and responsiveness to enhancers. In particular, P2 promoters contain built-in activating sequences that increase both enhancer and promoter activity, which seem to reduce their responsiveness to distal enhancers. This model for human promoters appears to differ qualitatively from previous studies of *Drosophila*, which found that the promoters of housekeeping and developmentally regulated genes can both be highly responsive, but to distinct sets of enhancer sequences and cofactors[9,20].

Together, these observations suggest a model in which the effects of enhancers on nearby genes in the human genome is controlled by quantitative tuning of intrinsic promoter activity, intrinsic enhancer activity and 3D enhancer–promoter contacts, with enhancer–promoter class compatibilities playing an additional but smaller part (Extended Data Fig. 10). Beyond these factors, further work will be required to identify and predict cases for which promoters are responsive only to certain chromatin environments, cofactors or enhancer sequences[3–8]. Regarding the latter possibility, other parallel studies have examined effects not explained by a multiplicative ExP model and found that combinations of TFs in enhancer and promoter sequences may mediate additional specificity[36,39].

A remaining challenge will be to link the sequences that control enhancer and promoter activities with effects on particular biochemical steps in transcription. In this respect, we found that GABPA and YY1 bind both to P2 promoters and to distal enhancers, and are associated with increased enhancer activity, increased promoter activity and reduced promoter responsiveness to distal enhancers. This suggests that distal enhancers may act, in part, on a particular rate-limiting step in transcription that can be saturated by the inclusion of built-in activating sequences in a gene promoter. Indeed, a previous study[35] found that adding GABPA and YY1 motifs to several promoters led to an increase in RNA expression that saturates at two or five copies of the motif, respectively. Given the preferred positions of these motifs within 20 bp of the TSS—as well as previous findings that these proteins physically interact with general TFs[42,43] and/or influence transcriptional initiation and TSS selection[37,44–46]—such a rate-limiting step might involve assembly of the preinitiation complex. In addition to this step, our data are consistent with a model in which enhancers and promoters control additional steps in transcription that multiplicatively combine and do not saturate in the dynamic range of our assay. Examples of such processes that could multiplicatively combine include control of burst frequency and burst size[47]. Further work will be required to investigate these possibilities.

Our study has several limitations that highlight areas for future work. First, the episomal STARR-seq assay does not capture all mechanisms that might influence transcriptional activation in the genome and may capture effects of sequences on other mechanisms, such as RNA stability[16,17,29]. Second, our experiments were not sufficiently powered to quantify possible compatibility among the weakest enhancers and promoters. Third, the exact proportions of variance explained by factors in the multiplicative model are influenced by the method of selecting enhancers and promoters for the experiment. Fourth, the extent to which promoter and enhancer classes might change across cell types is unclear. Further investigation with genome editing, orthogonal assays and additional cell types will be required to resolve these outstanding questions.

Together, our findings identified simple rules for human enhancer–promoter compatibility, which will propel efforts to model gene expression, map the effects of human genetic variation and design regulatory sequences for gene therapies.

Online content

Any methods, additional references, Nature Research reporting summaries, source data, extended data, supplementary information, acknowledgements, peer review information; details of author contributions and competing interests; and statements of data and code availability are available at https://doi.org/10.1038/s41586-022-04877-w.

1. ENCODE Project Consortium. An integrated encyclopedia of DNA elements in the human genome. *Nature* **489**, 57–74 (2012).
2. van Arensbergen, J., van Steensel, B. & Bussemaker, H. J. In search of the determinants of enhancer–promoter interaction specificity. *Trends Cell Biol.* **24**, 695–702 (2014).
3. Emami, K. H., Navarre, W. W. & Smale, S. T. Core promoter specificities of the Sp1 and VP16 transcriptional activation domains. *Mol. Cell. Biol.* **15**, 5906–5916 (1995).
4. Ohtsuki, S., Levine, M. & Cai, H. N. Different core promoters possess distinct regulatory activities in the *Drosophila* embryo. *Genes Dev.* **12**, 547–556 (1998).
5. Emami, K. H., Jain, A. & Smale, S. T. Mechanism of synergy between TATA and initiator: synergistic binding of TFIID following a putative TFIIA-induced isomerization. *Genes Dev.* **11**, 3007–3019 (1997).
6. Butler, J. E. F. Enhancer–promoter specificity mediated by DPE or TATA core promoter motifs. *Genes Dev.* **15**, 2515–2519 (2001).

7. Yean, D. & Gralla, J. Transcription reinitiation rate: a special role for the TATA box. *Mol. Cell. Biol.* **17**, 3809–3816 (1997).
8. Wefald, F. C., Devlin, B. H. & Williams, R. S. Functional heterogeneity of mammalian TATA-box sequences revealed by interaction with a cell-specific enhancer. *Nature* **344**, 260–262 (1990).
9. Zabidi, M. A., Arnold, C. D., Schernhuber, K. & Pagani, M. Enhancer–core-promoter specificity separates developmental and housekeeping gene regulation. *Nature* **518**, 556–559 (2015).
10. Banerji, J., Rusconi, S. & Schaffner, W. Expression of a β-globin gene is enhanced by remote SV40 DNA sequences. *Cell* **27**, 299–308 (1981).
11. Banerji, J., Olson, L. & Schaffner, W. A lymphocyte-specific cellular enhancer is located downstream of the joining region in immunoglobulin heavy chain genes. *Cell* **33**, 729–740 (1983).
12. Melnikov, A. et al. Systematic dissection and optimization of inducible enhancers in human cells using a massively parallel reporter assay. *Nat. Biotechnol.* **30**, 271–277 (2012).
13. Arnold, C. D. et al. Genome-wide quantitative enhancer activity maps identified by STARR-seq. *Science* **339**, 1074–1077 (2013).
14. Kermekchiev, M., Pettersson, M., Matthias, P. & Schaffner, W. Every enhancer works with every promoter for all the combinations tested: could new regulatory pathways evolve by enhancer shuffling? *Gene Expr.* **1**, 71–81 (1991).
15. Tewhey, R. et al. Direct identification of hundreds of expression-modulating variants using a multiplexed reporter assay. *Cell* **172**, 1132–1134 (2018).
16. Klein, J. C. et al. A systematic evaluation of the design and context dependencies of massively parallel reporter assays. *Nat. Methods* **17**, 1083–1091 (2020).
17. Muerdter, F. et al. Resolving systematic errors in widely used enhancer activity assays in human cells. *Nat. Methods* **15**, 141–149 (2018).
18. Nguyen, T. A. et al. High-throughput functional comparison of promoter and enhancer activities. *Genome Res.* **26**, 1023–1033 (2016).
19. Arnold, C. D. et al. Genome-wide assessment of sequence-intrinsic enhancer responsiveness at single-base-pair resolution. *Nat. Biotechnol.* **35**, 136–144 (2017).
20. Haberle, V. et al. Transcriptional cofactors display specificity for distinct types of core promoters. *Nature* **570**, 122–126 (2019).
21. Li, X. & Noll, M. Compatibility between enhancers and promoters determines the transcriptional specificity of gooseberry and gooseberry neuro in the *Drosophila* embryo. *EMBO J.* **13**, 400–406 (1994).
22. Fulco, C. P. et al. Activity-by-contact model of enhancer-promoter regulation from thousands of CRISPR perturbations. *Nat. Genet.* **51**, 1664–1669 (2019).
23. van Arensbergen, J. et al. Genome-wide mapping of autonomous promoter activity in human cells. *Nat. Biotechnol.* **35**, 145–153 (2017).
24. Wall, L., deBoer, E. & Grosveld, F. The human β-globin gene 3′ enhancer contains multiple binding sites for an erythroid-specific protein. *Genes Dev.* **2**, 1089–1100 (1988).
25. Tuan, D. Y., Solomon, W. B., London, I. M. & Lee, D. P. An erythroid-specific, developmental-stage-independent enhancer far upstream of the human "beta-like globin" genes. *Proc. Natl. Acad. Sci. USA* **86**, 2554–2558 (1989).
26. Thakore, P. I. et al. Highly specific epigenome editing by CRISPR–Cas9 repressors for silencing of distal regulatory elements. *Nat. Methods* **12**, 1143–1149 (2015).
27. Klann, T. S. et al. CRISPR–Cas9 epigenome editing enables high-throughput screening for functional regulatory elements in the human genome. *Nat. Biotechnol.* **35**, 561–568 (2017).
28. Fulco, C. P. et al. Systematic mapping of functional enhancer-promoter connections with CRISPR interference. *Science* **354**, 769–773 (2016).
29. Liu, Y. et al. Functional assessment of human enhancer activities using whole-genome STARR-sequencing. *Genome Biol.* **18**, 219 (2017).
30. Haberle, V. & Stark, A. Eukaryotic core promoters and the functional basis of transcription initiation. *Nat. Rev. Mol. Cell Biol.* **19**, 621–637 (2018).
31. Lenhard, B., Sandelin, A. & Carninci, P. Metazoan promoters: emerging characteristics and insights into transcriptional regulation. *Nat. Rev. Genet.* **13**, 233–245 (2012).
32. Fan, K., Moore, J. E., Zhang, X.-O. & Weng, Z. Genetic and epigenetic features of promoters with ubiquitous chromatin accessibility support ubiquitous transcription of cell-essential genes. *Nucleic Acids Res.* **49**, 5705–5725 (2021).
33. Xi, H. et al. Identification and characterization of cell type-specific and ubiquitous chromatin regulatory structures in the human genome. *PLoS Genet.* **3**, e136 (2007).
34. Landolin, J. M. et al. Sequence features that drive human promoter function and tissue specificity. *Genome Res.* **20**, 890–898 (2010).
35. Weingarten-Gabbay, S. et al. Systematic interrogation of human promoters. *Genome Res.* **29**, 171–183 (2019).
36. Sahu, B. et al. Sequence determinants of human gene regulatory elements. *Nat. Genet.* **54**, 283–294 (2022).
37. Yu, M. et al. GA-binding protein-dependent transcription initiator elements. Effect of helical spacing between polyomavirus enhancer a factor 3(PEA3)/ETS-binding sites on initiator activity. *J. Biol. Chem.* **272**, 29060–29067 (1997).
38. Curina, A. et al. High constitutive activity of a broad panel of housekeeping and tissue-specific *cis*-regulatory elements depends on a subset of ETS proteins. *Genes Dev.* **31**, 399–412 (2017).
39. Martinez-Ara, M., Comoglio, F., van Arensbergen, J. & van Steensel, B. Systematic analysis of intrinsic enhancer–promoter compatibility in the mouse genome. *Mol. Cell* https://doi.org/10.1101/2021.10.21.465269 (2022).
40. Maricque, B. B., Chaudhari, H. G. & Cohen, B. A. A massively parallel reporter assay dissects the influence of chromatin structure on cis-regulatory activity. *Nat. Biotechnol.* **37**, 90–95 (2019).
41. Hong, C. K. Y. & Cohen, B. A. Genomic environments scale the activities of diverse core promoters. *Genome Res.* **32**, 85–96 (2022).
42. Chiang, C. M. & Roeder, R. G. Cloning of an intrinsic human TFIID subunit that interacts with multiple transcriptional activators. *Science* **267**, 531–536 (1995).
43. Austen, M., Lüscher, B. & Lüscher-Firzlaff, J. M. Characterization of the transcriptional regulator YY1. The bipartite transactivation domain is independent of interaction with the TATA box-binding protein, transcription factor IIB, TAFII55, or cAMP-responsive element-binding protein (CPB)-binding protein. *J. Biol. Chem.* **272**, 1709–1717 (1997).
44. Sucharov, C., Basu, A., Carter, R. S. & Avadhani, N. G. A novel transcriptional initiator activity of the GABP factor binding ets sequence repeat from the murine cytochrome c oxidase Vb gene. *Gene Expr.* **5**, 93–111 (1995).
45. Carter, R. S. & Avadhani, N. G. Cooperative binding of GA-binding protein transcription factors to duplicated transcription initiation region repeats of the cytochrome c oxidase subunit IV gene. *J. Biol. Chem.* **269**, 4381–4387 (1994).
46. Usheva, A. & Shenk, T. YY1 transcriptional initiator: protein interactions and association with a DNA site containing unpaired strands. *Proc. Natl Acad. Sci. USA* **93**, 13571–13576 (1996).
47. Larsson, A. J. M. et al. Genomic encoding of transcriptional burst kinetics. *Nature* **565**, 251–254 (2019).
48. The FANTOM Consortium and the RIKEN PMI and CLST (DGT). A promoter-level mammalian expression atlas. *Nature* **507**, 462–470 (2014).

Publisher's note Springer Nature remains neutral with regard to jurisdictional claims in published maps and institutional affiliations.

© The Author(s), under exclusive licence to Springer Nature Limited 2022

Methods

Genome build

All analyses and coordinates are reported using human genome reference hg19.

Design of ExP STARR-seq

We designed ExP STARR-seq to systematically measure the intrinsic, sequence-encoded compatibility or specificity of many pairs of human enhancer and promoter sequences. The key design features we considered when developing this assay were the ability to measure the activity of individual enhancer–promoter sequence combinations, to precisely quantify the expression of each enhancer–promoter pair and to test hundreds of thousands of combinations to identify patterns of compatibility or specificity across a large number of human sequences.

Accordingly, we designed a new variant of the STARR-seq high-throughput plasmid reporter assay called ExP STARR-seq. In both STARR-seq and ExP STARR-seq, enhancer sequences are cloned downstream of a promoter, transfected into cells and transcribed to produce a reporter mRNA transcript, which is then sequenced to quantify the relative expression levels of plasmids containing different enhancer sequences[13]. In ExP STARR-seq, we modified the cloning and RNA-seq strategy to enable testing of different enhancer sequences in combination with different promoter sequences.

To clone combinations of enhancer and promoter sequences into a reporter plasmid, we synthesized 264 bp enhancer and promoter sequences in an oligonucleotide pool format, PCR amplified enhancer and promoter sequences separately and inserted them into the hSTARR-seq_SCP1 vector_blocking 4 vector[17] in the promoter position (replacing the original *SCP1* promoter) or enhancer position in a single pooled cloning step using Gibson assembly to generate all pairwise combinations of chosen enhancer and promoter sequences (Fig. 1a and Extended Data Fig. 1a). We chose this specific STARR-seq vector with four polyA sequences upstream of the promoter position because it was specifically designed to avoid spurious transcription initiation from the origin of replication[17], which would interfere with the STARR-seq signal from the cloned enhancer–promoter pairs. This STARR-seq vector also includes 5′ and 3′ splice sites upstream of the enhancer that allows the use of a PCR primer that targets the splice junction to specifically amplify cDNA derived from the reporter mRNA while avoiding amplifying the plasmid DNA sequence.

To quantify the reporter mRNA transcripts and determine which enhancer–promoter pair they correspond to, we further adapted the cloning and RNA-seq design. In the standard STARR-seq assay, the reporter mRNA contains the enhancer sequence but not the full promoter sequence, and therefore it cannot determine from which promoter a given reporter mRNA is derived. Accordingly, in ExP STARR-seq we introduced a random 16-mer sequence located immediately upstream of the enhancer sequence that we use as a plasmid barcode to identify which enhancer reporter mRNAs are derived from which enhancer–promoter pairs (Fig. 1a). After cloning the plasmid pool, we mapped which plasmid barcodes correspond to which promoters by applying Illumina high-throughput sequencing to a PCR amplicon that contains the promoter sequence and plasmid barcode. From this, we built a dictionary to look up, for a given reporter mRNA containing a plasmid barcode and enhancer sequence, which enhancer–promoter–plasmid barcode construct that mRNA is derived from.

Finally, we selected the number of constructed tested (about 1 million pairs of enhancer and promoter sequences cloned, with an average of 6.3 plasmid barcodes per pair) and sequencing depth (>1 billion reads per replicate) to enable highly precise measurements of expression for each enhancer–promoter pair. We obtained high reproducibility of enhancer–promoter expression levels between biological replicates ($R^2 = 0.92$), allowing us to develop quantitative models of how enhancer and promoter activities combine.

Altogether, this approach enabled precise quantification of the expression levels of thousands of combinations of enhancer and promoter sequences.

Selection of enhancer and promoter sequences for ExP STARR-seq

To explore the compatibility of human enhancers and promoters, we selected 1,000 promoter and 1,000 enhancer sequences, including sequences from the human genome spanning a range of expression or activity levels, and dinucleotide shuffled controls. Based on available lengths of oligonucleotide pool synthesis, each sequence was 264 bp.

For the promoters, we selected the 1,000 promoter sequences to include the following:

- 65 genes for which enhancers have previously been studied in CRISPR experiments in K562 cells[22].
- 715 genes sampled to span a range of potential promoter activities, including the 200 most highly expressed genes in K562 cells, based on the CAGE signal at their TSS[1] and a random sample of 515 other expressed genes (>1 transcripts per million (TPM) in RNA-seq data[28]).
- 20 genes that are not expressed or lowly expressed in K562 cells (<1 TPM), and that are expressed in both GM12878 and HCT-116 cells (in the top 70% of genes by TPM based on RNA-seq[1]).
- 100 random genomic sequences as negative controls (positive strand).
- 100 dinucleotide shuffles of these random genomic sequences.

For the selected genes, we synthesized a 264 bp sequence, including approximately 244 bp upstream and 20 bp downstream of the TSS. Here we defined the TSS as the centre of the 10-bp window with the most CAGE 5′ read counts within 1 kbp of a RefSeq TSS. For lowly expressed genes (which lack a clear CAGE signal), we used the hg19 RefSeq-annotated TSS. For genes studied in a previous study[22], we adjusted the assigned 10 bp TSS window by manual examination of the CAGE if necessary.

For the enhancers, we selected the 1,000 enhancer sequences to include the following:

- 131 elements previously studied using CRISPR[22], including (1) all distal elements (that is, >1 kb from an annotated TSS) with significant effects in previous CRISPRi tiling screens (activating or repressive), (2) all distal elements predicted by the ABC model to regulate one of the tested genes in K562 cells[22], and (3) two promoter elements for PVT1 that also act as enhancers for MYC[22]. We selected 264-bp regions centred on the overlapping DNase I hypersensitivity site (DHS) narrow peak. For the small number of CRISPR elements that did not overlap a narrow peak, we tiled the corresponding element with 264-bp windows overlapping by 50 bp.
- 200 DNase peaks with the strongest predicted enhancer activity, and 351 other DNase peaks sampled evenly across the range of predicted enhancer activity. Here we considered all distal DHS peaks in K562 cells (DHS narrow peaks[22]) and calculated predicted enhancer activity as the geometric mean of DHS and H3K27ac ChIP-seq read counts in K562 cells in the approximately 500 bp candidate enhancer regions used by the ABC model in a previous study[22]. Some candidate ABC elements in this set span more than one DHS peak, in which case we divided the predicted enhancer activity equally among each overlapping peak. We downloaded introns from the UCSC Genome Browser refGene track (v.2017-06-24) and removed any peaks overlapping an annotated splice donor or acceptor site. We then selected 264-bp regions centred on the remaining DHS narrow peaks.
- 100 random genomic sequences as negative controls.
- 100 dinucleotide shuffles of these random genomic sequences.

All enhancer sequences were taken from the hg19 reference in the positive strand direction.

Library cloning

We ordered 264 bp sequences in an oligonucleotide array format from Twist Bioscience with separate pairs of 18 bp adaptors (total length of

300 bp) for enhancers (5′ = GCTAACTTCTACCCATGC, 3′ = GCAAGTTAAG TAGGTCGT) and promoters (5′ = TCATGTGGGACATCAAGC, 3′ = GCATAGT GAGTCCACCTT). We then PCR amplified enhancers and promoters separately from the same array using Q5 high-fidelity DNA polymerase (NEB, M0492) (see Supplementary Table 10 for primer sequences). We amplified enhancers in four 50-µl PCR reactions (98 °C for 30 s; 15 cycles of 98 °C for 15 s, 61 °C for 15 s and 72 °C for 20 s) using primers (forward: TAGA TTGATCTAGAGCATGCANNNNNNNNNNNNNNNNGAGTACTGGTATGTT CAGCTAACTTCTACCCATGC, reverse: TCGAAGCGGCCGGCCGAATTCGTC ATTCCATGGCATCTCACGACCTACTTAACTTGC), which add an additional 17 bp on either side, a 16 bp N-mer plasmid barcode upstream and homology arms for Gibson assembly on either side of the enhancer sequence. For the motif ExP STARR-seq experiment, we used 18 cycles of PCR for amplifying the enhancers. We amplified promoters in four 50 µl PCR reactions (98 °C for 30 s; 4 cycles of 98 °C for 15 s, 61 °C for 15 s, 72 °C for 20 s; 11 cycles of 98 °C for 15 s and 72 °C for 20 s) using primers (forward: CTCTGGCCTAACTGGCCGGTACGAGTGAGCTCTCGTTCA TCATGTGGGA CATCAAGC, reverse: CCCAGTGCCTCACGACCGGGCCTGGTAGCAAGC TTAGATAAGGTGGACTCACTATGC), which add an additional 17 bp and homology arms for Gibson assembly on either side of the promoter sequence. For the motif ExP STARR-seq experiment, we used 4 and 14 cycles of PCR for amplifying the promoters. We purified the PCR products using 0.8× volume of AMPure XP beads (Beckman Coulter, A63881) and pooled the reactions together while keeping enhancers and promoters separate.

We digested the human STARR-seq screening vector (hSTARR-seq_ SCP1 vector_blocking 4, Addgene, 99319) with both Thermo SgrDI and BshTI (AgeI) (replaced with enhancer sequence), then NEB KpnI and ApaI (replaced with promoter sequence), with purification using 0.8× volume AMPure XP after each digestion. We then recombined 500 ng of this digestion (including about 4.4 kb of backbone vector and 250 bp of filler sequence, including a spliced region and truncated GFP open reading frame) with 150 ng of both the purified enhancer and promoter products using Gibson assembly (NEB, E2611) for 1 h at 50 °C in a 40 µl reaction. The reaction was purified using 1× volume AMPure XP with 3 total ethanol washes.

We electroporated the assembled libraries into Lucigen Endura electrocompetent cells (60242) using 0.1 cm cuvettes (Bio-Rad) and a Gene Pulser Xcell Microbial system (Bio-Rad) (10 µF, 600 Ω, 1,800 V) following the manufacturer's recommendations. We expanded the transformations for 12 h in LB medium with carbenicillin while also estimating the number of transformed colonies by plating a serial dilution of transformation mixture as previously described[49]. We midi-prepped the expanded transformations with a ZymoPURE II Plasmid Midiprep kit (D4200) or with a Nucleobond Xtra Midiprep kit from Macherey-Nagel (for the motif ExP STARR-seq experiment).

Building the barcode–promoter dictionary

We introduced a unique 16 bp plasmid barcode adjacent to the enhancer sequence to enable us to determine from which promoter each transcript originated, which, together with the self-transcribed enhancer, allowed us to map each transcript to a promoter–enhancer pair.

To build the map from 16 bp plasmid barcodes to promoters, we PCR amplified a fragment containing both the promoter and plasmid barcode from the plasmid library (98 °C for 1 min; 16 cycles of 98 °C for 10 s, 66 °C for 15 s and 72 °C for 25 s; ExP_P1_fwd_I2: AATGAT ACGGCGACCACCGAGATCTACAC[index-2]GGGAGGTATTGGACAGGC, ExP_P3_rev: CAAGCAGAAGACGGCATACGAGATGCATGGGTAGAAGTT AGCTGAAC) and sequenced the promoter position with paired-end reads (using the custom sequencing primers ExP_P1_fwd_seq_R1: GAGTGAGCTCTCGTTCATCATGTGGGACATCAAGC, ExP_P2_rev_seq_R2: TGGTAGCAAGCTTAGATAAGGTGGACTCACTATGC) and the plasmid barcode with an index read (using the custom sequencing primer ExP_ fwd_BC_seq: GTCCCAATTCTTGTTGAATTAGATTGATCTAGAGCATGCA). We mapped these sequences to a specially constructed index of the promoter sequences using bowtie2 (X: -q -met-stderr -maxins 2000 -p 4 -no-mixed -dovetail -fast). We dropped any barcod–promoter pairs with singleton reads, then removed ambiguous pairings (more than one promoter for the same barcode), and finally thresholded pairs with at least five reads to build the barcode–promoter dictionary.

Cell culture

We maintained K562 erythroleukaemia cells (American Type Culture Collection) at a density between 100,000 and 1,000,000 cells per ml in RPMI-1640 (Thermo Fisher Scientific) with 10% heat-inactivated FBS, 2 mM L-glutamine and 100 units per ml streptomycin and 100 mg ml^{-1} penicillin by diluting cells 1:8 in fresh medium every 3 days. Cell lines were regularly tested for mycoplasma and authenticated through analysis of RNA-seq and ATAC-seq data.

Library transfection

We nucleofected 10 million K562 cells with 15 µg of the ExP plasmid library in 100 µl cuvettes with a Lonza 4D-Nucleofector using settings and protocols specified by the manufacturer for K562 cells (T-016). We pooled 5 nucleofections together during recovery to form 50 million cell biological transfection replicates and generated 4 replicates for a total of 200 million cells. After 24 h, we collected the cells in Qiagen buffer RLT (79216) and proceeded with STARR-seq library preparation. For the motif ExP STARR-seq experiment, we collected 6.5–10 million nucleofected cells per replicate.

STARR-seq library preparation

We proceeded with STARR-seq library preparation using an adapted protocol[13]. We split the 50 million cell transfection replicates in half and extracted total RNA using three Qiagen RNeasy mini columns (74134), performing the on-column DNase step. We isolated polyA+ mRNA using a Qiagen Oligotex mRNA kit for the 1,000 × 1,000 ExP dataset (note this kit has been discontinued, we now use the Poly(A) Purist MAG kit from Thermo Fisher Scientific, AM1922). Following mRNA elution, TURBO DNase (Thermo Fisher Scientific, AM2238) was added in 100 µl reactions and incubated at 37 °C for 30 min, then another 2 µl of TURBO DNase was added and incubated at 37 °C for 15 min. We purified the RNA following DNA digestion with Zymo RNA Clean & Concentrator 5 (R1013) (R1018 for the motif ExP STARR-seq experiment). We reverse-transcribed the polyA+ mRNA using Thermo SuperScriptIV using the STARR_RT primer (CAAACTCATCAATGTATCT TATCATG) in 20 µl reactions according to the manufacturer's recommendations. We included 1 µl of the ribonuclease inhibitor RNaseOUT (Invitrogen, 10777019). Following reverse transcription, we added 1 µl of RNaseH (Thermo Fisher Scientific, EN0201) and incubated at 37 °C for 20 min. We purified the cDNA with 1.8× volume of AMPure XP beads. We selectively amplified the reporter transcript using intron-spanning junction primers with Q5 polymerase in 50 µl reactions (98 °C for 45 s; 15 cycles of 98 °C for 15 s, 65 °C for 30 s and 72 °C for 70 s, jPCR_fwd: TCGTGAGGCACTGGGCAG*G*T*G*T*C, jPCR_rev: CTTATCATGTCTGCTCGA*A*G*C, where the asterisk represents phosphorothioate bonds). Following purifications with 0.8× volume of AMPure XP beads, we performed a test final sequencing-ready PCR with a dilution of the junction PCR product to determine the optimal cycle number, then proceeded with the final PCR using Q5 polymerase in 50 µl reactions (98 °C for 45 s; about 9 cycles of 98 °C for 10 s, 65 °C for 30 s and 72 °C for 30 s, ExP_GFP_fwd_I2: AATGATACGGCGACCACC GAGATCTACAC[index-2]GGCTTAAGCATGGCTAGCAAAG, ExP_P4_rev: CAAGCAGAAGACGGCATACGAGATTCATTCCATGGCATCTCACG. For the 1,000 × 1,000 ExP STARR-seq experiment, we purified the final libraries with 2 rounds of 0.8× volume of SPRISelect (Beckman Coulter, B23318) (1 round of 0.7× SPRISelect for the motif ExP STARR-seq experiment).

Alignment and counting of STARR-seq data

To characterize activity in the STARR-seq assay, we defined STARR-seq expression for a given plasmid (corresponding to a particular promoter,

enhancer and plasmid barcode) as the expression of the reporter RNA transcript normalized to the abundance of that plasmid in the input DNA pool.

To quantify STARR-seq expression, we sequenced the library of RNA transcripts produced from replicate transfections (described above) along with the DNA input with paired-end reads (using the custom sequencing primers ExP_P3_fwd_seq_R1: GAGTACTGGTATG TTCAGCTAACTTCTACCCATGC, ExP_P4_rev_seq_R2: TCATTCCATGG CATCTCACGACCTACTTAACTTGC) and the plasmid barcode with an index read (using the custom sequencing primer ExP_fwd_BC_seq: GTCCCAATTCTTGTTGAATTAGATTGATCTAGAGCATGCA). We aligned reads for both the RNA and DNA libraries to the designed enhancer sequences using bowtie2 (bowtie2 options: -q -met 30 -met-stderr -maxins 2000 -p 16 -no-discordant -no-mixed -fast).

We counted reads separately from PCR replicates derived from each biological replicate of 50 million transfected cells, and scaled each of the PCR replicates within a biological replicate such that they had the same total normalized counts, equal to the maximum across all PCR replicates. We combined counts into per-biological replicate counts for further processing. We used the barcod–promoter dictionary to identify the promoter associated with each transcript. We used the same mapping and barcode–promoter assignment process for DNA.

For subsequent analysis, we discarded plasmids that had fewer than 25 DNA reads or fewer than 1 RNA transcript reads from further processing.

Computing technical reproducibility and influence of plasmid barcode sequences

To assess the technical reproducibility of ExP-STARR-seq, we first compared STARR-seq expression between biological replicate experiments. Specifically, we first combined data from biological replicates 1 and 2 and replicates 3 and 4. Next, we correlated $\log_2$(RNA/DNA) for these groups before (Fig. 1b and Extended Data Fig. 1b) and after (Extended Data Fig. 1e,f), averaging across plasmid barcodes corresponding to the same enhancer–promoter pair.

We next assessed the variation between plasmids with the same enhancer and promoter sequences but different random 16 bp plasmid barcodes, because these 16 nucleotides of random sequence might contain TF motifs or other sequences that affect STARR-seq expression. To do so, we combined data from all biological replicate experiments and created two virtual replicates for each enhancer–promoter pair by splitting the corresponding plasmid barcodes into two groups. For example, an enhancer–promoter pair with six plasmid barcodes was split into two virtual replicates each with three barcodes). We averaged $\log_2$(STARR-seq expression) within enhancer–promoter pairs (across different barcodes) and correlated these virtual replicates. We compared versions of this analysis for increasing thresholds on the minimum number of barcodes in each virtual replicate (Extended Data Fig. 1e,f).

Estimating enhancer and promoter activities using the naive averaging approach

We sought to compare the intrinsic activities of different enhancer and promoter sequences in ExP STARR-seq—that is, the contribution of a given enhancer or promoter sequence to STARR-seq expression relative to other sequences. We estimated enhancer activity and promoter activity in two ways: by a simple averaging method and by fitting a multiplicative Poisson count model (see next section).

As a first approach to estimate promoter activity, we calculated, for each promoter sequence, the average $\log_2$(STARR-seq expression) when that promoter is paired with random genomic sequences in the enhancer position (Fig. 1c). This quantity represents the basal (or autonomous) expression level of the promoter in the absence of a strong activating sequence in the enhancer position.

As an initial approach to estimate enhancer activity, we calculated, for each enhancer sequence, the average $\log_2$(STARR-seq expression) of all pairs including that enhancer sequence (Fig. 1d).

As noted above, we fit this model on the set of plasmids with at least 25 DNA reads, and at least 1 RNA read. In addition, to reduce noise in our promoter and enhancer activity estimates, we required at least two separate plasmid barcodes per promoter–enhancer pair. These filters resulted in 604,268 promoter–enhancer pairs across 4,512,907 total unique plasmids (approximately 7.5 plasmids per pair) that were used to estimate promoter and enhancer activity.

In practice, this averaging method of calculating enhancer and promoter activity was inaccurate and biased for several reasons. First, the averaging method does not consider the variance introduced by sampling and counting noise in sequencing, which is significant because many promoter–enhancer pairs have low RNA read counts. Second, the averaging method does not account for differences introduced due to missing data. In the 1,000 enhancer × 1,000 promoter data matrix, many entries are missing either due to low RNA counts (resulting from counting and sampling noise or from low expression) or due to low DNA counts (resulting from variation introduced in cloning the plasmid library). As a result of these factors, the averaging method produces biased (inflated) estimates of activity for weaker enhancer and promoter sequences because the expression of plasmids containing these sequences is more likely to drop below the threshold of detection given our sequencing depth (Extended Data Fig. 2c,d).

Because this model explained the data well, we used this same model to estimate intrinsic enhancer and promoter activity.

Estimating intrinsic enhancer and promoter activities using the multiplicative model

We fit a count-based Poisson model to address the limitations of using a simple averaging approach to estimate intrinsic enhancer and promoter activities (see previous section) and to quantify the extent to which the ExP STARR-seq data can be explained by a simple multiplicative function of intrinsic enhancer and promoter activities. In this multiplicative model, all enhancers are assumed to activate all promoters by the same fold-change without enhancer–promoter interaction terms.

Specifically, we estimated enhancer and promoter activities from ExP STARR-seq data by fitting the observed RNA read counts to a multiplicative function of observed DNA input read counts, intrinsic enhancer activity and intrinsic promoter activity as follows:

$$\mathrm{RNA} \sim \mathrm{Poisson}(k \times \mathrm{DNA} \times P \times E),$$

where P is the intrinsic promoter activity of the promoter sequence p, E is intrinsic enhancer activity of the enhancer sequence e, and k is a global scaling/intercept term that accounts for factors that control the relative counts of DNA and RNA, such as sequencing depth.

We fit these parameters using block coordinate descent on the negative log-likelihood of the distribution above, initially fixing $k = 0$, then alternatively optimizing promoter activities while holding enhancer activities constant, and enhancer activities while holding promoter activities constant.

We then re-normalized enhancer activities and promoter activities by the mean activity of random genomic sequences and adjusted the scaling factor k accordingly.

In practice, this model produces similar estimates to simply taking the mean value of an enhancer sequence across all promoters and vice versa, but accounts for missing data points in the 1,000 × 1,000 matrix and provides a more robust estimate for very weak enhancers or promoters, which produce relatively little RNA and are therefore difficult to measure in this STARR-seq experiment, except when paired with a strong element in the other group (Extended Data Fig. 2c,d).

Assessing a multiplicative model for gene expression in the genome

We tested whether gene transcription in the genome could be modelled as a multiplicative function of promoter activity and enhancer

inputs. To measure gene transcription, we applied PRO-seq as previously described[50] to K562 cells to map transcriptionally engaged RNA polymerase, and assigned gene transcription as reads per kilobase per million in the gene body, excluding the region within 1 kb of the annotated TSS. To estimate promoter activity, we used the intrinsic promoter activity estimate from ExP STARR-seq. To estimate enhancer input, we summed the ABC scores for all nearby enhancers (within 5 Mb of the TSS). The ABC scores in turn are estimated on the basis of multiplying enhancer activity (geometric mean of DHS and H3K27ac ChIP-seq read counts at an enhancer) by enhancer–promoter contact frequency (estimated from Hi-C data)[51]. We considered all genes with 'active' promoters, defined as those with DHS and H3K27ac signals above the 40th percentile of all genes in the genome as used in the ABC model[51].

Computing and clustering residuals from the multiplicative model

We explored whether enhancer–promoter compatibility could explain the variation in STARR-seq expression beyond that explained by the multiplicative model. To do so, we looked for shared behaviours between groups of promoters and enhancers by clustering them according to their residual error from the Poisson model described above. For each enhancer–promoter pair, we used the Poisson model above to compute predicted RNA given the input DNA counts and estimates of intrinsic enhancer and promoter activities. We then computed a transformed residual as $\log_2$(predicted RNA + psuedocount) − $\log_2$(observed RNA + psuedocount), where pseudocount = 10 to stabilize variance of the estimates across the range of values for RNA[52]. We filtered to all enhancer–promoter pairs with at least two barcodes and calculated the mean of the residuals across barcodes to form a (sparse) 1,000 × 1,000 matrix of residuals indexed by promoter and enhancers.

We clustered this matrix independently along rows and columns (treating missing pairs as having a residual of 0) using *K*-means with 3 clusters, labelling the clusters as 0, 1 and 2 such that they had increasing mean activity estimates in the Poisson model. One cluster each of enhancers and promoters (E0 and P0) contained sequences that were missing many data points owing to their weaker activity, which led to dropout owing to low RNA expression. The sparsity of data for the E0 and P0 clusters prevented accurate characterization of compatibility; therefore, we excluded these clusters from subsequent analysis.

Assessing reproducibility of the clusters

We evaluated whether the clustering we observed in the residuals was a general trend of the data or an artefact of a few promoters or enhancers. To test this possibility, we randomly downsampled the residual matrix to 25% of promoters and 25% of enhancers (6.25% of the total data) 100 times and clustered the subsets. The original (full data) cluster identity of a promoter or enhancer predicted the downsampled cluster with greater than 80% accuracy (Extended Data Fig. 4f).

Estimating enhancer activity with specific promoter classes and promoter responsiveness to specific enhancer classes

We evaluated whether certain promoters were more responsive when paired with different enhancer classes, and whether certain enhancers had more activity when paired with promoters from different classes (Fig. 3c,d).

To explore differences in enhancer activity when paired with different promoter classes, we fit the Poisson model (described above) separately to two different subsets of the data: (1) all enhancer sequences paired with P1 or genomic background promoter sequences (producing an estimate of the activity of an enhancer sequence on a P1 promoter); and (2) all enhancer sequences paired with P2 or genomic background promoter sequences (producing an estimate of the activity of an enhancer sequence on a P2 promoter).

Similarly, to estimate promoter responsiveness to either E1 or E2 enhancers, we fit the Poisson model to the subsets: (3) all promoters paired with E1 or genomic background enhancer sequences (producing an estimate of the responsiveness of a promoter sequence to E1 enhancers): and (4) all promoters paired with E2 or genomic background enhancer sequences (producing an estimate of the responsiveness of a promoter sequence to E2 enhancers).

We used the genomic background promoter sequences to set a common baseline.

Annotating enhancer and promoter sequences with genomic features and sequence motifs

To annotate enhancer and promoter sequences with features of TF binding of the corresponding genomic elements, we downloaded list of human TF ChIP-seq narrowpeak files from the ENCODE Project[1] and annotated each enhancer or promoter sequence with the maximum signalValue column for any overlapping peak (or 0 signal for no overlap). We then compared the fold-change in signal between classes of sequences (Fig. 4d, Extended Data Fig. 6a and Supplementary Table 11).

To annotate enhancer and promoter sequences with TF motifs, we used FIMO[53] (default parameters, including *P* value threshold of 10^{-4}) to identify matches for HOCOMOCO v.11 CORE motifs[54]. We then compared the fold-change in motif counts between classes of sequences (Extended Data Figs. 6b,c and 7l and Supplementary Tables 5 and 7).

For comparing features between E1 and E2 enhancers, we compared motif, ChIP-seq and other features between the E1 and E2 enhancer sequences that overlapped the summit of a DNase peak.

For analysing the proportion of P2 promoters bound by various factors, we defined 'strongly bound' as having a ChIP-seq signal greater than 20% of maximum ChIP-seq signal among P1 and P2 promoters.

Logistic regression to classify P1 and P2 promoters

We trained a logistic regression classifier to distinguish P1 versus P2 promoters and to classify all promoters genome-wide as P1 or P2 (Supplementary Table 8). We used as input sequence and genomic features as described above. To standardize features with varying distributions, we removed features with non-zero values in fewer than five promoters, normalized continuous TF binding and histone mark features with respect to DNase activity, and performed hyperbolic arcsine transformation on all continuous features.

Owing to redundancy of the ENCODE TF ChIP-seq data and highly similar motifs between certain TFs, many features were highly correlated. To address this, we constructed an undirected weighted graph in which vertices are features and edges are defined by the Pearson correlation coefficient between two features. After removing edges with weights of less than 0.8, we treated each connected component in the graph as a distinct feature. Most resulting connected components contained only one feature, whereas highly correlated redundant features were grouped into one connected component. For connected components with more than one feature, we collapsed the features into one by taking the average. In total, we used 2,535 features for model training.

We then trained an elastic net logistic regression model to classify P1 and P2 promoters using 80% of the data. We ranked features with non-zero model coefficients and selected top features based on an elbow-point cut-off. We then retrained a model using this smaller set of features to mitigate overfitting, which resulted in 145 final features. The model achieved 94% mean accuracy across sixfold cross validation.

We applied this model to all gene promoters in the genome (Supplementary Table 8). As expected, we observed marked functional difference between genes with predicted P1 and P2 promoters, whereby nearly all ribosomal subunits (82 out of 84) are predicted to be P2 promoters and, more broadly, 78% of previously annotated housekeeping genes were predicted to have P2 promoters.

Assessing cell-type specificity of gene expression across cell types and tissues

We analysed CAGE data from the FANTOM5 consortium across 1,829 experiments (biosamples)[30]. We downloaded expression data (in TPM)

from https://fantom.gsc.riken.jp/5/datafiles/latest/extra/gene_level_expression/hg19.gene_phase1and2combined_tpm.osc.txt.gz on 19 February 2022. We defined ubiquitously expressed genes as genes that are expressed at ≥1 TPM in ≥95% of biosamples. We defined uniformly versus variably expressed genes as genes for which maximum expression is less than (or greater than) 10 times the median expression across biosamples, respectively.

Comparison of CRISPR-derived regulatory elements for P1 versus P2 promoters

To compare the number and effect sizes of genomic regulatory elements for P1 and P2 promoters, we analysed CRISPRi tiling screens from previous studies that perturbed all DNase-accessible sites around selected genes[22,27,28]. We counted the number of activating distal regulatory elements—that is distal, non-promoter DNase-accessible sites for which perturbation led to a significant reduction in gene expression (Fig. 4c). We also compared the effect sizes on gene expression for these same activating distal regulatory elements (Extended Data Figs. 6e and 7e).

Luciferase assays

We tested the ability of each of seven large *MYC* enhancer fragments to activate the promoters of three genes in the *MYC* locus—*MYC*, *PVT1* and *CCDC26*—using a classical plasmid luciferase-based enhancer assay. The seven *MYC* enhancers were defined as the 1.0–2.2 kb sequences identified in our previous *MYC* proliferation-based CRISPRi screen[28], and a 1 kb bacterial plasmid sequence was used as a negative control sequence. We cloned promoter fragments into plasmids in combination with each of these sequences (Supplementary Table 3). The promoter fragments corresponded to the dominant TSS of each gene in K562 cells (as determined by CAGE). For *PVT1* and *CCDC26*—which do not appear to be regulated by most of the seven *MYC* enhancers in the genome—we cloned two promoter fragments of different lengths to determine whether nearby sequences might encode biochemical specificity. We designed an insertion site about 1 kb upstream of the promoter in the plasmid for inserting each enhancer sequence (Extended Data Fig. 3a), and we flanked this region with polyadenylation signals in either direction to avoid measuring luciferase activity driven from transcripts initiating from the enhancer elements themselves. Luciferase assays using a Dual-Luciferase Reporter assay (Promega) were performed as previously described[28] in four to six biological replicates. For each experiment, we calculated the fold-change in luciferase signal (firefly/*Renilla*) for enhancer versus negative control (Extended Data Fig. 3c).

Assessing the cell-type specificity of E1 and E2 enhancers

We tested whether E1 and E2 enhancer sequences from ExP STARR-seq overlapped elements predicted to act as enhancers by the ABC model in K562 cells or in 128 other cell types and tissues. To do so, we intersected the E1 and E2 enhancer sequences with the approximately 200-bp regions predicted by the ABC model to act as enhancers for at least 1 nearby expressed gene, as previously defined[51]. The ABC enhancer–gene predictions from this previous study[51] are available at https://www.engreitzlab.org/resources/.

Aligning promoters by TSS

For each 264 bp promoter sequence, we defined the primary TSS as the nucleotide with the highest stranded 5′ signal in GRO-Cap data in K562 cells (Gene Expression Omnibus identifier GSM1480321)[55]. This primary TSS position was used for plotting genomic signals relative to the TSS and in analyses of motif positioning (for example, for GABPA and YY1).

Analysis of motif position relative to TSS

We used FIMO[53] to scan for HOCOMOCO motifs in promoters, including for GABPA (GABPA_HUMAN.H11MO.0.A), YY1 (TYY1_HUMAN.H11MO.0.A) and the TATA box (TBP_HUMAN.H11MO.0.A). We report positional preferences as the distance between the primary TSS from GRO-cap (see above) and the centre of the motif. For example, for GABPA, the most common position was −10 relative to the TSS (that is, with the second 'G' in the core 'GGAA' motif located at position −10).

HS-STARR-seq to measure enhancer activity for millions of genomic sequences

We conducted two STARR-seq experiments to measure the enhancer activity of millions of long genomic sequences tiling across human enhancer and promoter sequences. To generate these tiling sequences, we used a hybrid selection strategy, similar to previous approaches[56]. Specifically, we purified genomic DNA from K562 cells, tagmented DNA using Tn5 and gel size selection to a size range of approximately 300–700 bp (Extended Data Fig. 8e), and conducted hybrid selection using RNA probes as previously described[50] targeting either (1) all gene promoters (HS promoter pool) or (2) all accessible elements (HS-accessible element pool) in K562 cells (see Supplementary Table 12 and Supplementary Table 13 for probe sequences). We amplified these sequences using primers that included a UMI (CapStarrFa_N10 primer: tagatTGAtCTAGAGCATGCACCGGCAAGCAGAAGACGGCATACGAGAT NNNNNNNNNNATGTCTCGTGGGCTCGGAGATGT and CapStarrR primer: CGAAGCGGCCGGCCGAATTCGTCGATCGTCGGCAGCGTCA GATGTG) and cloned these selected sequences into the hSTARR-seq_ori vector[17], which uses the bacterial origin of replication (ORI) sequence as the promoter for the reporter transcript, by Gibson assembly. In the final HS promoter and accessible element pools, 9% and 12% of fragments mapped to their intended targets, respectively, and each element was tiled by a median of 20 and 55 sequences, respectively. We conducted the rest of the STARR-seq experiment as described above, transfecting 50 million cells per replicate for 4 replicates.

We sequenced the input DNA libraries to a depth of 880 million and 810 million reads (promoter and accessible element pools, respectively), and the RNA libraries to a depth of 1.1 billion reads (both pools). We aligned reads to the hg19 genome using bowtie2 (options: -q -met-stderr -maxins 1000 -p 4 -no-discordant -no-mixed). We discarded fragments with fewer than 25 aligned DNA reads. Biological replicates were highly correlated (R^2 = 0.92 and 0.91 for promoter and accessible element pools, respectively) (Extended Data Fig. 8d).

We analysed this dataset by computing a $\log_2$(activity per fragment) equal to the $\log_2$(RNA/DNA) and correcting for a fragment-length bias. We noted that STARR-seq expression was highly inversely correlated with the length of the enhancer sequence, even among random genomic fragments that did not overlap putative regulatory elements, which could result from biases in library preparation and sequencing. To adjust for this, we fit a linear regression (separately for the two pools) and subtracted this regression from the $\log_2$(RNA/DNA) activity to give a bias-corrected activity. We then correlated motifs with bias-corrected activity. To estimate enhancer activity of promoters from the ExP, we found HS-STARR-seq fragments that overlapped at least 90% of an ExP promoter and averaged their activity scores.

Analysis of variance

Analysis of variance (ANOVA) results were computed on the basis of intrinsic activities, and represent the sequential sum of squares (type I ANOVA) analyses. For example, in Extended Data Fig. 2j,k, we calculated the proportion of variance explained by promoters, the proportion of variance explained by enhancers after controlling for promoter activity, the proportion of variance explained by class interactions after controlling for promoter and enhancer activity, and, finally, any remaining variance.

Motif ExP STARR-seq library design

For the motif-insertion experiment, we selected 15 promoters from the P1 and P2 promoter clusters that had also been previously studied[22],

and with intrinsic activities between −2 and +2 (evenly spaced sampling from promoters ordered by intrinsic activity). We included a weak promoter in each cluster (intrinsic activity less than −3) and included the promoters for GATA1 and RPL37A (two other weak promoters).

We selected 15 enhancers from each of the E1 and E2 enhancer clusters, from elements detected as endogenous enhancers in K562 cells in a previous study[22], with intrinsic activity between −2 and 2 (evenly spaced sampling from enhancers ordered by intrinsic activity), and avoiding potential polyA signals in the enhancer sequence. We added one weak enhancer from each class (intrinsic activity less than −3), and one weak scramble enhancer sequence from the original experiment.

To explore the effect of adding GABPA, YY1, or other motifs to promoters, in every promoter sequence selected above, we inserted 2 copies of the GABPA consensus motif, centred at −10 and −31 relative to the TSS (identified by CAGE) to generate a new promoter sequence. For each original sequence, we did the same with YY1 at +1 relative to the TSS. Consensus motifs were taken from the HOCOMOCO v11 CORE motifs[54].

To explore the effect of breaking motifs in promoters, for each promoter sequence selected above, we identified any GABPA or YY1 motifs (FIMO[53], default parameters, including *P* value threshold of 10^{-4}, motifs within 30 bases of the TSS), and swapped 2 bases in the core of the motifs (for example, GGAAG to GAGAG in GABPA motifs, and ATGGC to AGTGC in YY1 motifs). For each original promoter sequence with more than one motif, we included a new promoter sequence with each individual motif modified, as well as a one new promoter sequence combining each of these modifications.

To explore the effect of adding GABPA motifs to enhancers, we inserted 2, 4, or 6 copies of the GAPBA consensus motif (GAACCG GAAGTGG) spaced by 21 bp to a single random background enhancer.

In this experiment, each originally selected promoter was also included in the enhancer sequence pool, and all enhancer sequences were included in both orientations in the plasmid. Promoter and enhancer sequences used in this experiment are listed in Supplementary Tables 14 and 15.

Motif ExP STARR-seq analysis

For the motif ExP STARR-seq experiment, we followed the methods detailed for the original STARR-seq experiment, but with the following exceptions. We sequenced the promoter DNA pool to a depth of 214.8 million reads. For the construction of the barcode–promoter dictionary, we initially aligned the promoter sequence reads to a specially constructed index of the unedited promoter sequences, using bowtie2 as described for the original STARR-seq experiment but with a slightly relaxed alignment threshold (X: -score-min L,−0.7,−0.7). We then used a custom Python script to check aligned reads at the sites of potential edits. The script reassigned a read to an edited promoter sequence if it perfectly matched the edited sequence at all edit positions and the immediate upstream and downstream base pair. If the read did not perfectly match an edited sequence but also did not match the wild-type sequence at the edit positions, the read was discarded. Reads with <90% perfect match with the entire sequence to which they were assigned were discarded. From this point, we returned to the original STARR-seq methods, namely dropping barcode–promoter pairs with singleton reads, removing ambiguous pairings and thresholding pairs with at least five reads to build the barcode–promoter dictionary.

We sequenced the pool consisting of two replicates of the input DNA library as well as four replicates of the RNA library to a total of 345.5 million reads. When quantifying STARR-seq expression, unlike with the original STARR-seq experiment, we sequenced two replicates of the input DNA library. Therefore, to quantify the DNA read count for the $\log_2$(RNA/DNA) calculation, we used the average count of the two replicates, weighted to the same total read count. STARR-seq expression was highly correlated across replicates (minimum $R^2 = 0.92$; Extended Data Fig. 9a). As with the original STARR-seq experiment, we only included in the final analysis plasmids that had greater than 25 DNA reads and greater than 1 RNA transcript, for a total of 362,905 plasmids across 19,019 promoter–enhancer pairs, with an average of 19 barcodes per pair (Extended Data Fig. 9b). For unedited promoter and enhancer pairs, the STARR-seq expression was highly correlated with the expression in the original ExP STARR-seq experiment (Extended Data Fig. 9c).

For edited promoters, to determine the change in responsiveness to E1 enhancers (Fig. 5e), we estimated unedited and edited responsiveness to E1 enhancers as described for the original experiment. We transformed the values out of $\log_2$(space) and computed the per cent change in the responsiveness as the per cent difference between the responsiveness of the edited sequence and the responsiveness of the unedited sequence.

For edited enhancers, to determine changes in enhancer activity with P1 and P2 promoters (Extended Data Fig. 9d), we calculated an inferred enhancer strength for each enhancer within a given enhancer–promoter pair as the ExP score for the pair minus the intrinsic promoter strength as calculated with the multiplicative model described above. We transformed these strength estimates out of $\log_2$(space) and then determined the per cent change in enhancer strength for each pair as the inferred strength of the edited enhancer with a given promoter minus the inferred strength of the unedited enhancer with the same promoter divided by the strength of the unedited enhancer. We then compared the change in enhancer strength for each edit type with all P1 promoters compared with P2 promoters using a two-tailed *t*-test.

Analysis of mouse embryonic stem cell MPRA experiments

Data from a previous study[39] were filtered to plasmids with at least five total DNA reads, and at least one RNA read in each of three replicates. Promoter–enhancer pairs were filtered to those with at least two barcodes. We estimated intrinsic promoter and enhancer activities using the same method as described above for the ExP-STARR multiplicative model, but without the final steps centring the activities of promoter and enhancer fragments from the genomic background to zero-strength.

Analysis and plotting tools

Data were processed and plotted using bowtie2 (v.2.3.4.1)[57], R (v.4.0.2)[58], Python (v.3.63)[59], numpy (v.1.17.4)[60], scipy (v.1.5.4)[61], pandas (v.1.1.5)[62], matplotlib (v.3.3.4)[63], seaborn (v.0.11.0)[64], scikit-learn (v.0.21.3)[65], ncls (v.0.051)[66] and statsmodels (v.0.12.2)[67].

Reporting summary

Further information on research design is available in the Nature Research Reporting Summary linked to this paper.

Data availability

Raw and processed data for ExP STARR-seq, motif ExP STARR-seq, HS-STARR-seq and K562 PRO-seq can be found at the NCBI's Gene Expression Omnibus under accession number GSE184426. Luciferase data can be found in Supplementary Table 3. Datasets used from the ENCODE Project are listed in Supplementary Table 10 and are available at https://www.encodeproject.org. Additional resources and protocols related to this study are available at https://www.engreitzlab.org/resources/.

Code availability

Code for fitting the multiplicative ExP model is available at https://doi.org/10.5281/zenodo.6514733 or https://github.com/broadinstitute/ExP-model-fit.

49. Wang, T., Lander, E. S. & Sabatini, D. M. Large-scale single guide RNA library construction and use for CRISPR–Cas9-based genetic screens. *Cold Spring Harb. Protoc.* **2016**, db.top086892 (2016).
50. Engreitz, J. M. et al. Local regulation of gene expression by lncRNA promoters, transcription and splicing. *Nature* **539**, 452–455 (2016).

51. Nasser, J. et al. Genome-wide enhancer maps link risk variants to disease genes. *Nature* **593**, 238–243 (2021).
52. Anscombe, F. J. The transformation of Poisson, binomial and negative-binomial data. *Biometrika* **35**, 246–254 (1948).
53. Grant, C. E., Bailey, T. L. & Noble, W. S. FIMO: scanning for occurrences of a given motif. *Bioinformatics* **27**, 1017–1018 (2011).
54. Kulakovskiy, I. V. et al. HOCOMOCO: towards a complete collection of transcription factor binding models for human and mouse via large-scale ChIP-seq analysis. *Nucleic Acids Res.* **46**, D252–D259 (2018).
55. Core, L. J. et al. Analysis of nascent RNA identifies a unified architecture of initiation regions at mammalian promoters and enhancers. *Nat. Genet.* **46**, 1311–1320 (2014).
56. Vanhille, L. et al. High-throughput and quantitative assessment of enhancer activity in mammals by CapStarr-seq. *Nat. Commun.* **6**, 6905 (2015).
57. Langmead, B. & Salzberg, S. L. Fast gapped-read alignment with Bowtie 2. *Nat. Methods* **9**, 357–359 (2012).
58. The R Development Core Team. *R: A Language and Environment for Statistical Computing* (R Foundation for Statistical Computing, 2014).
59. Van Rossum, G. & Drake, F. L. *Python 3 Reference Manual*. (CreateSpace, 2009).
60. Harris, C. R. et al. Array programming with NumPy. *Nature* **585**, 357–362 (2020).
61. Virtanen, P. et al. SciPy 1.0: fundamental algorithms for scientific computing in Python. *Nat. Methods* **17**, 261–272 (2020).
62. McKinney, W. Data structures for statistical computing in Python. In *Proc. 9th Python in Science Conference* (eds van der Walt, S. & Millman, J) 51–56 (SciPy, 2010).
63. Hunter, J. D. Matplotlib: a 2D graphics environment. *Comput. Sci. Eng.* **9**, 90–95 (2007).
64. Waskom, M. seaborn: statistical data visualization. *J. Open Source Softw.* **6**, 3021 (2021).
65. Pedregosa, F. et al. Scikit-learn: machine learning in Python. *J. Mach. Learn. Res.* **12**, 2825–2830 (2011).
66. Stovner, E. B. & Sætrom, P. PyRanges: efficient comparison of genomic intervals in Python. *Bioinformatics* **36**, 918–919 (2020).
67. Seabold, S. & Perktold, J. Statsmodels: econometric and statistical modeling with Python. in *Proc. 9th Python in Science Conference* (eds van der Walt, S. & Millman, J) 92–96 (SciPy, 2010).

Acknowledgements This work was supported by a NHGRI Genomic Innovator Award (R35HG011324 to J.M.E.); Gordon and Betty Moore and the BASE Research Initiative at the Lucile Packard Children's Hospital at Stanford University (J.M.E.); a NIH Pathway to Independence Award (K99HG009917 and R00HG009917 to J.M.E.); the Harvard Society of Fellows (J.M.E.); the Novo Nordisk Foundation Center for Genomic Mechanisms of Disease (J.M.E.); the Broad Institute (E.S.L.); an AΩA Carolyn L. Kuckein Student Research Fellowship (D.T.B.); NHGRI Ruth L. Kirschstein NRSA Predoctoral Institutional Research Training Grants (T32HG000044, V.L.); and by the National Institute of General Medical Sciences (T32GM007753, L.S.). We thank B. van Steensel and M. Martinez-Ara for sharing data and discussing analysis. We thank C. Vockley, V. Subramanian and members of the Engreitz and Lander research groups for discussions and technical assistance. E.S.L is currently on leave from the Broad Institute, MIT, and Harvard.

Author contributions D.T.B., C.P.F., T.R.J., J.R. and J.M.E. developed the ExP STARR-seq assay. D.T.B., J.R., M.K., A.R. and T.H.N. performed the STARR-seq experiments. M.K. performed the luciferase assay experiments. D.T.B., T.R.J., V.L., E.J., L.S., H.Y.K., J.N., S.R.G. and J.M.E. analysed the STARR-seq data. M.K. and J.M.E analysed the luciferase assay data. E.S.L. and J.M.E. supervised the work. All authors contributed to writing the manuscript.

Competing interests C.P.F. is now an employee and shareholder of Bristol Myers Squibb. J.M.E. is a shareholder of Illumina, Inc, and other biotechnology companies. All other authors declare no competing interests.

Additional information

Supplementary information The online version contains supplementary material available at https://doi.org/10.1038/s41586-022-04877-w.

Correspondence and requests for materials should be addressed to Jesse M. Engreitz.

Peer review information *Nature* thanks Alex Nord and the other, anonymous, reviewer(s) for their contribution to the peer review of this work.

Reprints and permissions information is available at http://www.nature.com/reprints.

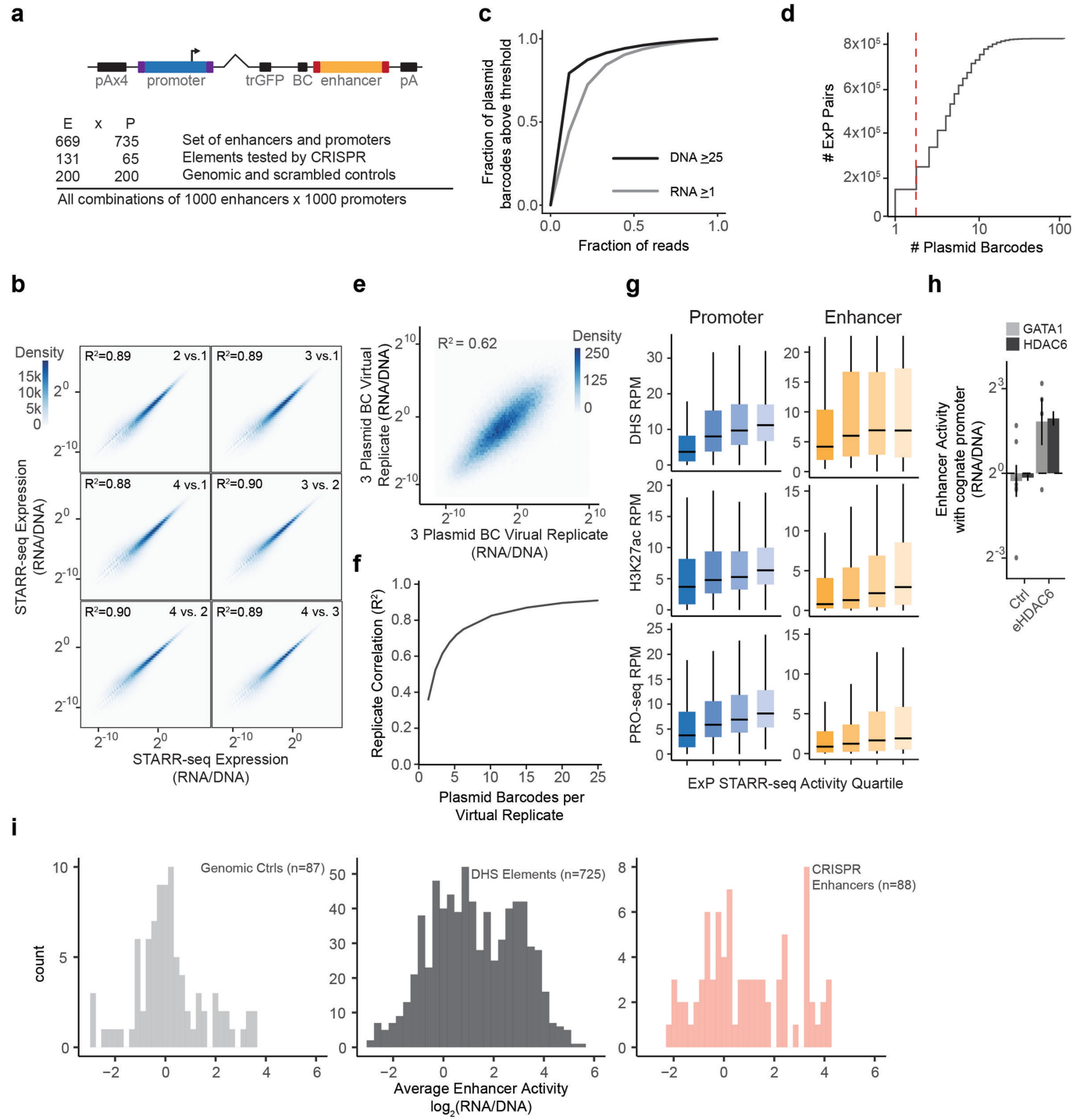

Extended Data Fig. 1 | Design and reproducibility of ExP STARR-seq. a. ExP STARR-seq reporter construct (pA = polyadenylation signal; purple = promoter sequencing adaptors; angled = spliced sequence; trGFP = truncated GFP open reading frame with start and stop codon; BC = 16 bp N-mer plasmid barcode; red = enhancer sequencing adaptors) and 1000x1000 K562 library contents. **b**. Correlation of ExP STARR-seq expression between biological replicate experiments, calculated for individual enhancer-promoter pairs with unique plasmid barcodes. Axes represent the average STARR-seq expression (RNA/DNA) of individual biological replicates. Density: number of enhancer-promoter plasmids. **c**. Fraction of remaining enhancer-promoter plasmids passing DNA (≥25) and RNA (≥1) threshold (y-axis) with downsampling of sequencing reads (x-axis). **d**. Distribution of plasmid barcodes per enhancer-promoter pair, red dotted-line is threshold of two plasmid barcodes. **e**. Correlation between virtual replicates, formed by sampling two nonoverlapping groups of three plasmid barcodes from pairs with at least 6 barcodes, and averaging $\log_2$(RNA/DNA) within groups. **f**. Correlation between virtual replicates as in (**c**) for increasing numbers of plasmid barcodes per pair in virtual replicates. **g**. DNase-seq, H3K27ac ChIP-seq, and PRO-seq (RPM) by increasing quartile of autonomous promoter activity and average enhancer activity in ExP STARR-seq (n = 800). Box: median and interquartile range (IQR). Whiskers: +/− 1.5 x IQR. **h**. Activation in ExP STARR-seq (expression versus genomic controls in distal position) of GATA1 and HDAC6 promoters by eHDAC6 (chrX:48641342-48641606). Ctrl = activity of promoters with random genomic controls in enhancer position. Error bars: 95% CI across plasmid barcodes. n = 7 (GATA1-ctrl), 381 (HDAC6-ctrl), 4 (eHDAC6-GATA1), 37 (eHDAC6-HDAC6). **i**. Average enhancer activity (STARR-seq expression of plasmids containing a given enhancer averaged across all promoters) of enhancer sequences derived from random genomic controls (n = 87), accessible elements (n = 725), and genomic enhancers validated in CRISPR experiments (n = 89).

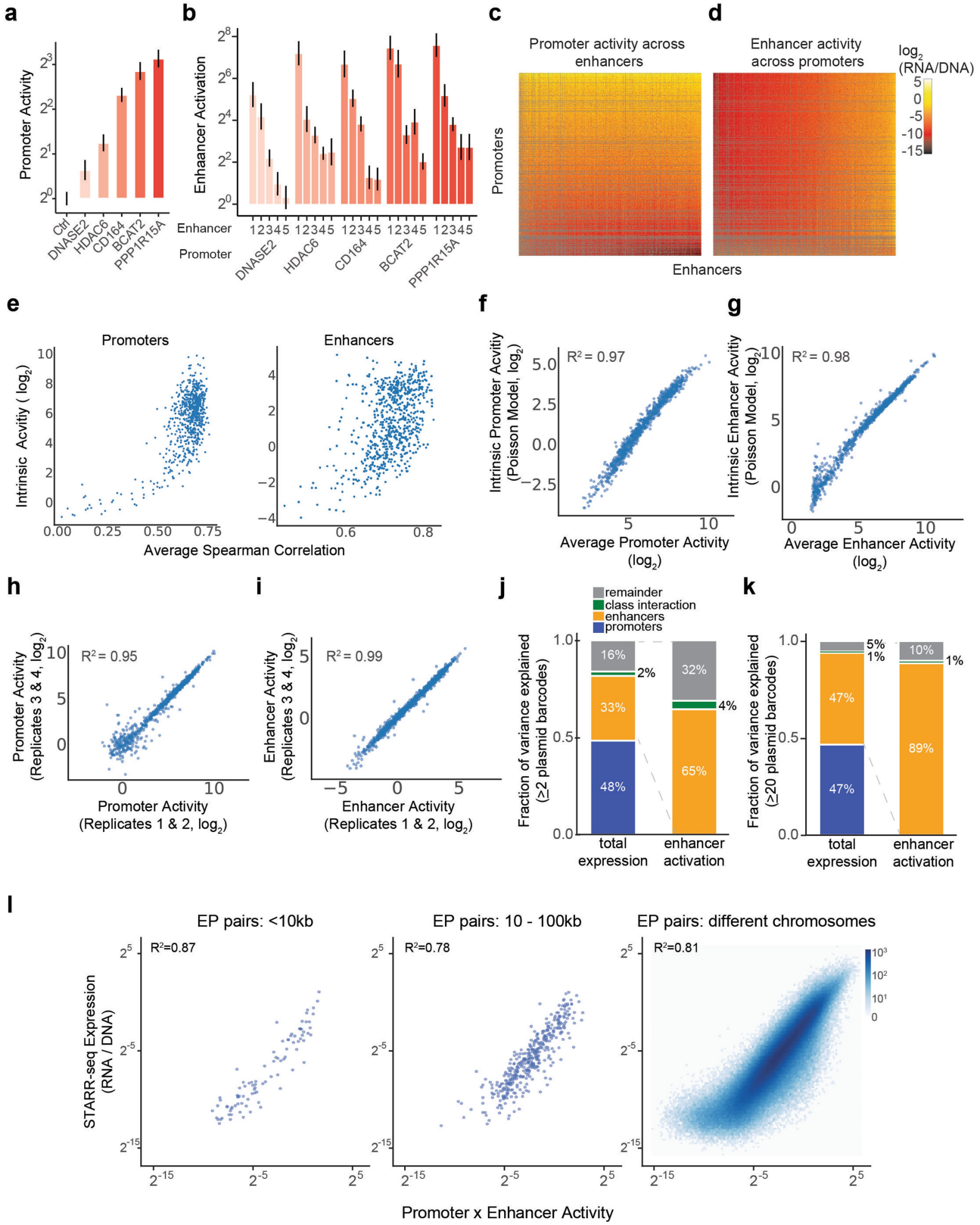

Extended Data Fig. 2 | See next page for caption.

Extended Data Fig. 2 | Comparison of methods of estimating enhancer and promoter activities and the multiplicative model. a. Intrinsic promoter activity (expression versus random genomic controls in enhancer position) of five selected promoters. Error bars: 95% CI across plasmid barcodes (n = 54-79). Promoter classes (see Methods): DNASE2 (P1), HDAC6 (P1), CD164 (P1), BCAT2 (P1), PPP1R15A (P2). **b**. Activation (expression versus random genomic controls in enhancer position) of 5 selected promoters by 5 selected enhancers: 1 = chr11:61602148-61602412 (E1), 2 = chr19:49467061-49467325 (E1), 3 = chrX:48641342-48641606 (E1), 4 = chr19:12893216-12893480 (E2), 5 = chr17:40851134-40851398 (E1). Error bars: 95% CI across plasmid barcodes (n = 12-56). **c**-**d**. Heatmap of promoter activity (**a**, expression divided by intrinsic enhancer activity) or enhancer activity (**b**, expression divided by intrinsic promoter activity) across all pairs of promoter (vertical) and enhancer sequences (horizontal). Axes are sorted by intrinsic promoter and enhancer activities, as in Fig. 2j. Grey: missing data. **e**. Intrinsic promoter and enhancer activity (y-axis, estimated by a Poisson count model) versus average pairwise Spearman correlation (as in Fig. 2c, d). **f**–**g**. Correlation between two estimates of promoter (**c**) and enhancer (**d**) activities. One method ("average activity", x-axis) estimates activity calculated by averaging across elements, and the other method ("intrinsic activity", y-axis) estimates activity by using coefficients estimated by a Poisson count model (see Methods). **h**–**i**. Correlation of intrinsic promoter (**e**) and enhancer (**f**) activity estimates from Poisson model using data from separate replicate experiments. **j**–**k**. Fraction of variance explained by promoter activity, enhancer activity, class interaction from the perspective of expression (STARR-seq score) and enhancer activation (fold-activation of an enhancer on a promoter, normalizing out promoter strength) limited to pairs with 2 or more (**c**) or 20 or more (**d**) plasmid barcodes. Plot includes pairs with P0 promoters and E0 enhancers. Bar plots show sequential sum of squares (Type-I ANOVA). **l**. Correlation of the multiplicative enhancer x promoter model with STARR-seq expression comparing enhancer-promoter pairs located within 10 kb, 100 kb, and pairs located on different chromosomes.

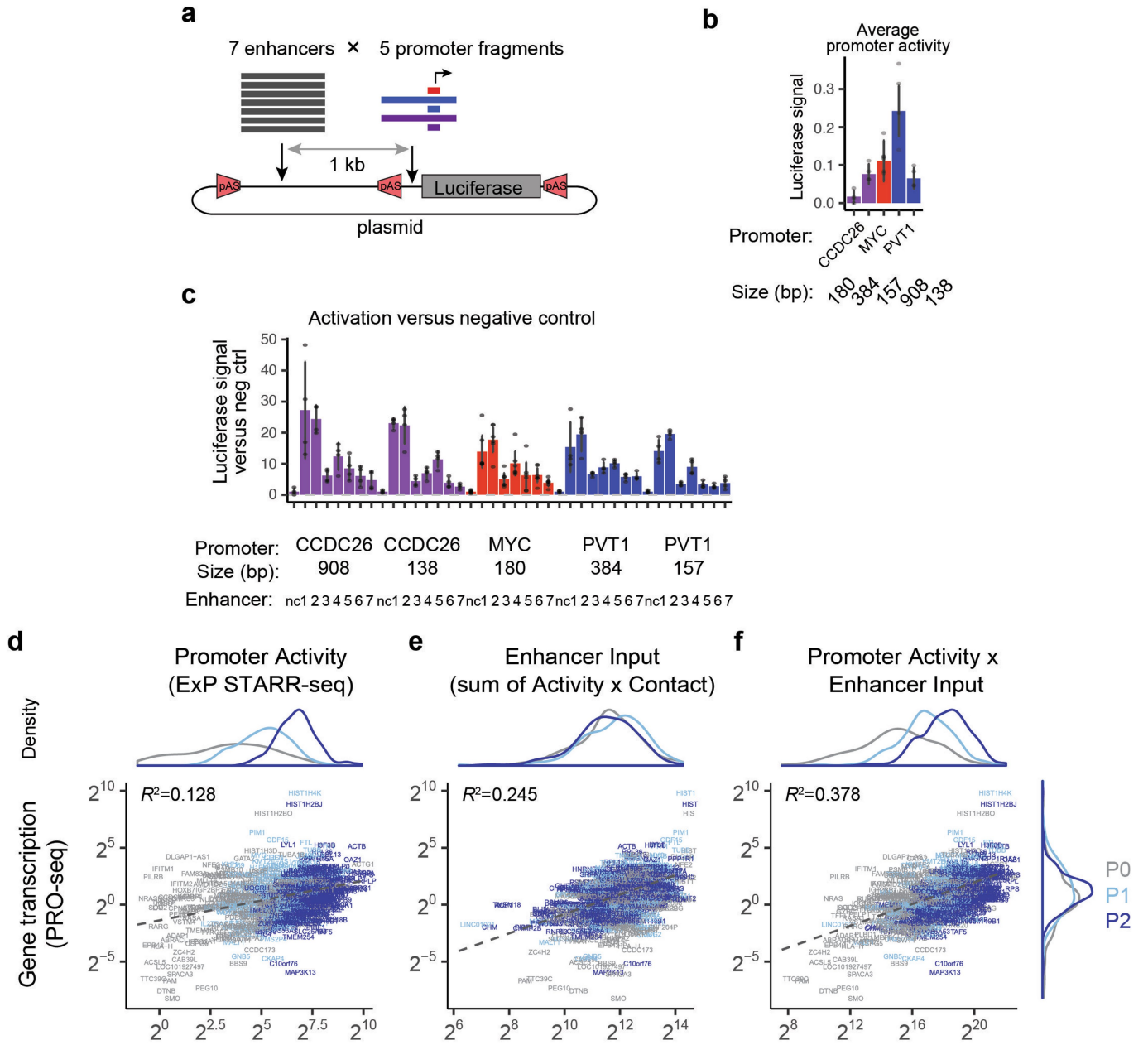

Extended Data Fig. 3 | Validation of enhancer-promoter multiplication via luciferase assays and modeling gene transcription as a function of intrinsic promoter activity and enhancer inputs. a. ExP luciferase reporter construct. Seven enhancer fragments, with flanking polyadenylation signals, were cloned upstream of five promoter fragments and measured via the dual luciferase assay. **b**. Autonomous promoter activity of ExP luciferase (average luciferase signal of promoter with negative control) for 5 promoter sequences derived from 3 genes (*MYC*, *PVT1*, *CCDC26*). Error bars are 95% CI from 6 (MYC) or 4 (all other promoters) biological replicates. **c**. Enhancer activation (luciferase signal versus negative control sequence in the enhancer position) of seven enhancers across five promoter fragments. Error bars are 95% CI from 6 (MYC) or 4 (all other promoters) biological replicates. **d-f**. Gene transcription (y-axis): PRO-seq read counts in the gene body. **a**. Promoter Activity (x-axis, left): Intrinsic promoter activity, as measured by ExP STARR-seq. **b**. Enhancer Input (x-axis, center): enhancer activity (based on measurements of H3K27ac and DHS in the genome) multiplied by enhancer-promoter contact (based on Hi-C measurements), summed across all putative enhancers (DHS peaks) within 5 Mb of the gene promoter (excluding the promoter's own peak), weighted by HiC contact as in the ABC Model[22]. **c**. Promoter Activity x Enhancer Input (x-axis, right). Labels: gene symbols for 741 promoters with sequence activity estimates from ExP STARR-seq and enhancer input estimates from ABC. Dotted lines: Line of best fit from linear regression in $\log_2$ space.

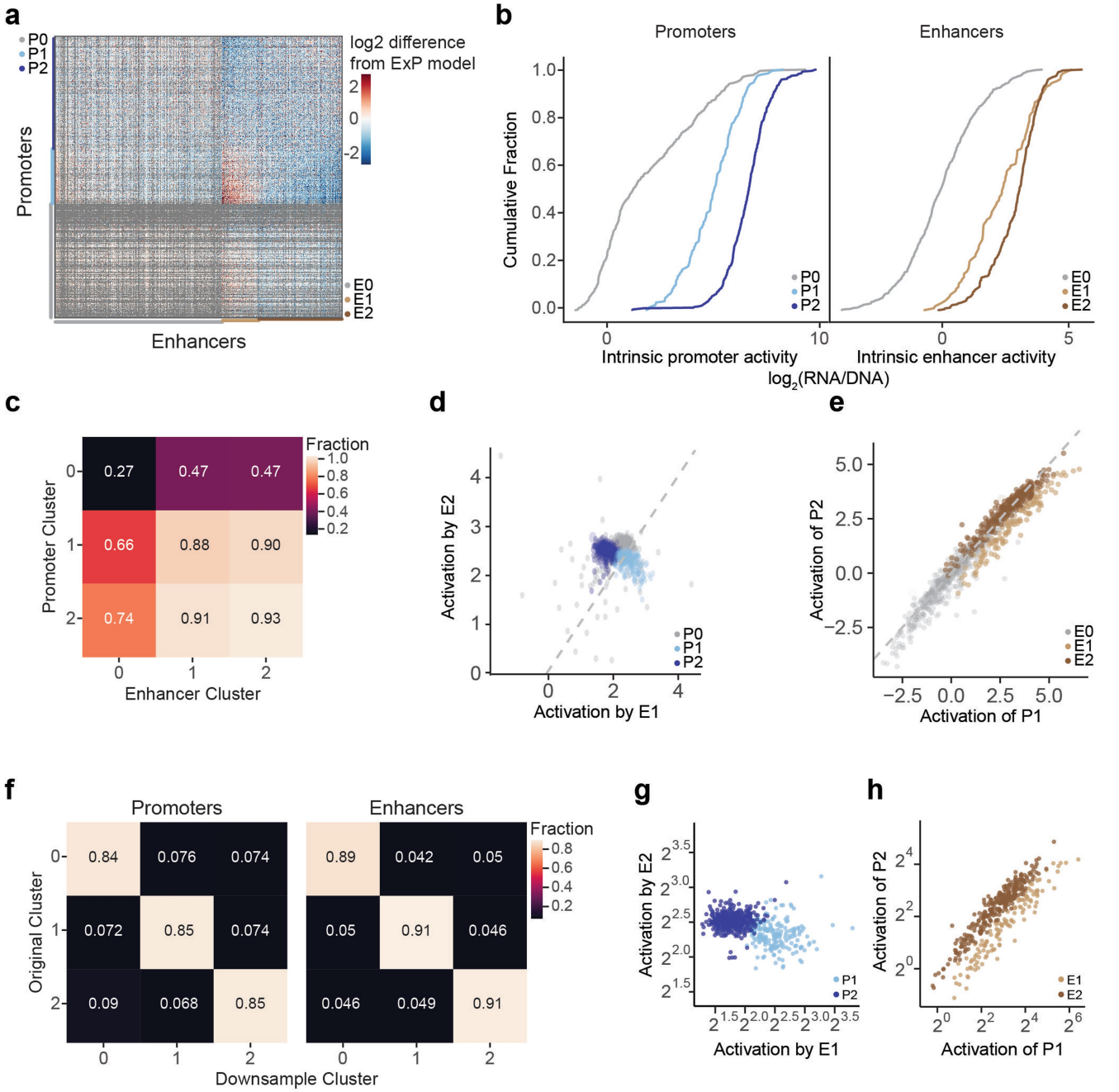

Extended Data Fig. 4 | Enhancer and promoter cluster identification and reproducibility. a. Heatmap of deviations in enhancer-promoter STARR-seq expression from a multiplicative enhancer-promoter model (color scale: fold-difference between observed expression versus expression predicted by multiplicative model; gray: missing data). Same as Fig 3a, except including clusters with weak sequences and missing data (E0 and P0). Vertical axis: promoter sequences grouped by class and sorted by responsiveness to E1 vs. E2; horizontal axis: enhancer sequences grouped by class and sorted by activation of P1 vs. P2. **b**. Distribution of intrinsic enhancer and promoter activity (expression versus genomic controls) by cluster. **c**. Fraction of enhancer-promoter pairs observed in ExP STARR-seq dataset (>= 2 plasmid barcodes) by cluster. **d**. Correlation of average promoter activation (expression versus genomic controls in enhancer position) by E2 versus E1 enhancer sequences. Each point is one promoter sequence. Same as Fig. 3c, except including P0 promoter sequences. **e**. Correlation of average activation of P2 versus P1 promoters. Each point is one enhancer sequence. Same as Fig. 3d, except including E0 enhancer sequences. **f**. Robustness of enhancer and promoter cluster assignments to downsampling of enhancer and promoter sequences. Clustering was repeated in 100 random downsamplings to 25% of promoter sequences and 25% of enhancer sequences (6.25% of original matrix). Heatmap: Average fraction overlap between cluster assignments from the full and downsampled matrices. **g**. Correlation of average promoter activation (expression versus genomic controls in enhancer position) by E2 versus E1 enhancer sequences using 'average activity' instead of model estimates. Each point is one promoter sequence. **h**. Correlation of average activation of P2 versus P1 promoters using 'average activity' instead of model estimates. Each point is one enhancer sequence.

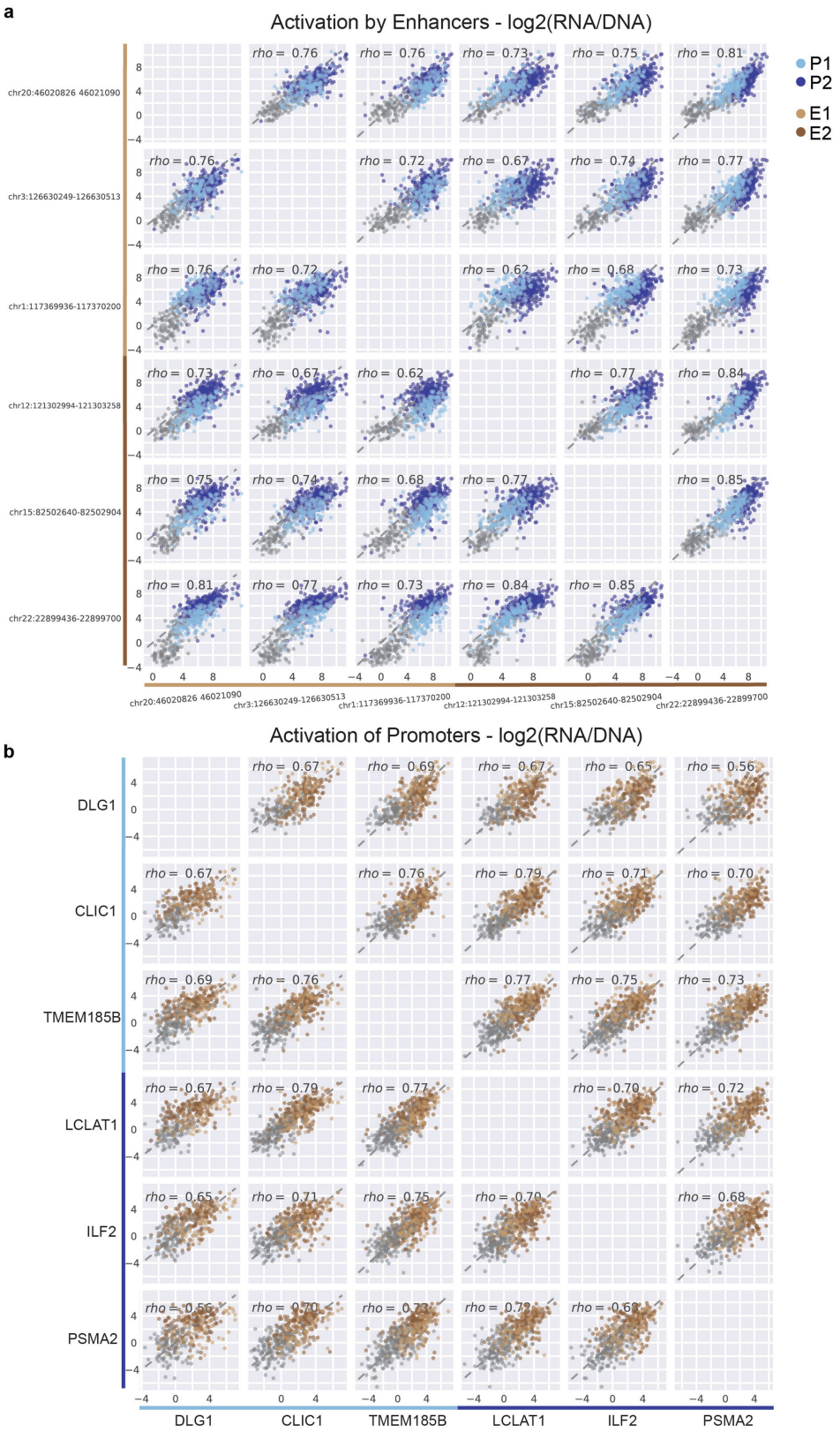

Extended Data Fig. 5 | Classes of enhancer and promoter sequences show distinct patterns of activation and responsiveness. a. For 6 representative enhancer sequences (3 E1 and 3 E2 sequences), the pairwise correlation of promoter activation (expression versus genomic controls in promoter position, averaged across plasmid barcodes). Each point is one promoter sequence. **b.** For 6 representative promoter sequences (3 P2 and 3 P1 sequences), the pairwise correlation of activation by enhancers (expression versus genomic controls in enhancer position, averaged across plasmid barcodes). Each point is one enhancer sequence.

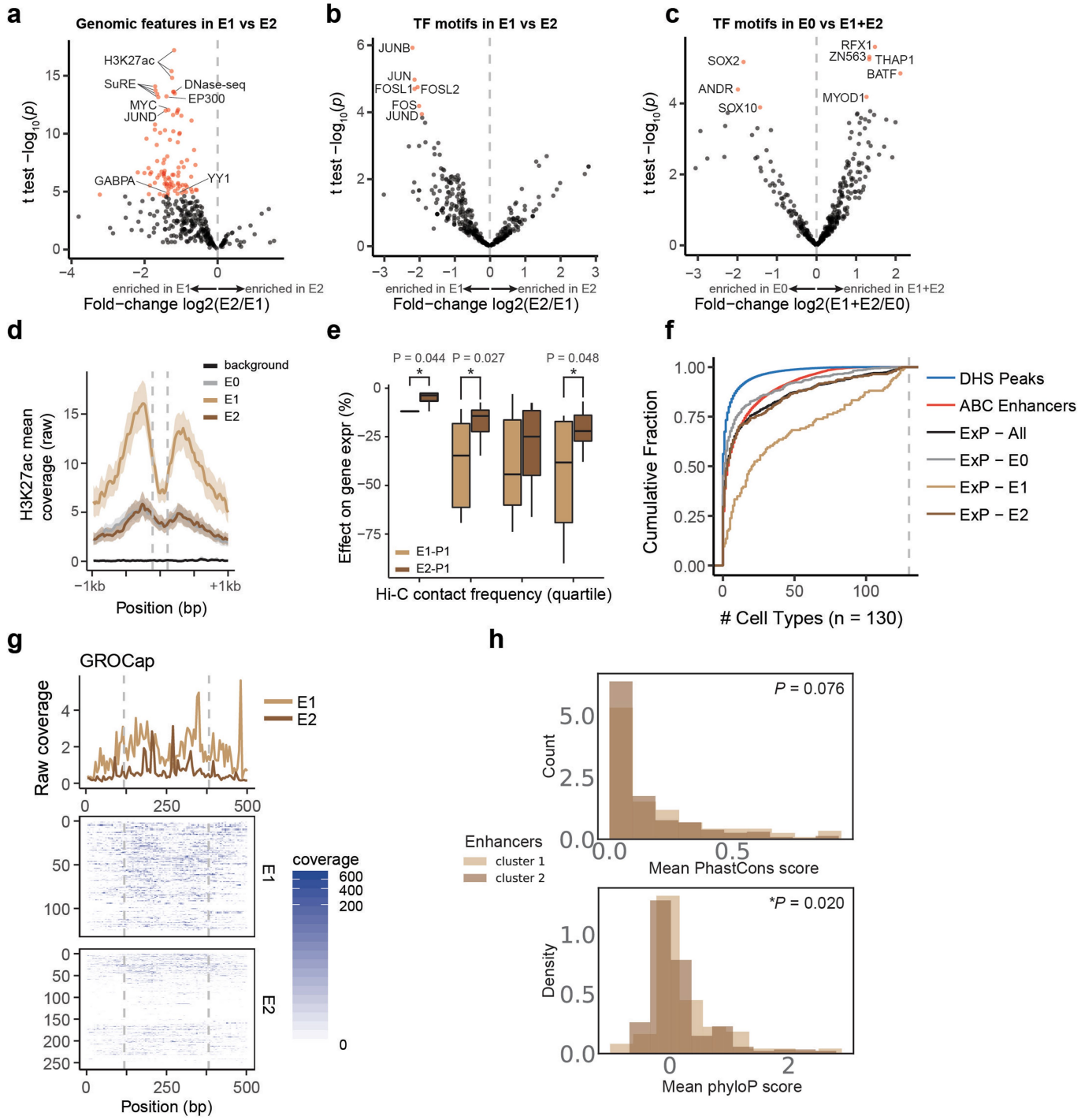

Extended Data Fig. 6 | See next page for caption.

Extended Data Fig. 6 | Classes of enhancer sequences correspond to strong and weak genomic enhancers. a. Volcano plot comparing ChIP-seq and other genomic features for E2 versus E1 enhancer sequences (see Supplementary Table 4). X-axis: ratio of average signal at P2 versus P1 promoters. Red dots: features with significantly higher signal at E1; no features have significantly higher signal at E2 enhancer sequences. **b**. Volcano plot comparing transcription factor motifs for E1 versus E2 enhancer sequences (see Supplementary Table 5). X-axis: ratio of average motif counts in E1 and E2 enhancer sequences. Red dots: Motifs significantly more frequent in E1 vs. E2 sequences. **c**. Volcano plot comparing transcription factor motifs for E1 and E2 versus E0 enhancer sequences (see Supplementary Table 5). X-axis: ratio of average motif counts in E1 and E2 versus E0 sequences. Red dots: Motifs significantly more frequent in E1 and E2 versus E0 sequences (>0) or more frequent in E0 versus E1 and E2 (<0). **d**. Mean H3K27ac ChIP-seq coverage of genomic elements corresponding to E0, E1, E2, or genomic control enhancer sequences (+/− 95% CI), aligned by DHS peak summit. Dotted lines mark bounds of the enhancer sequences used in ExP STARR-seq. E0 and E2 distributions are overlapping. **e**. % effect of genomic elements corresponding to E1 vs. E2 enhancer sequences on expression of genes corresponding to P1 promoters in CRISPRi screens, separated by quartiles of 3D contact frequency measured by Hi-C (0.39-11.9 (n = 9), 11.9-23.9 (n = 31), 23.9-58.3 (36), 58.3-100(n=34)). **P* < 0.05, two-sample, two-sided *t*-test. Boxes are median and interquartile range, whiskers are +/− 1.5*IQR. **f**. Cumulative density plot showing the cell-type specificity of enhancer sequences selected for ExP STARR-seq, and DNase peaks or ABC enhancers in K562 cells. X-axis: # of cell types other than K562 in which the element is predicted to be an ABC enhancer. **g**. GRO-Cap coverage of genomic enhancers used in ExP STARR-seq. Top: Mean coverage of enhancers corresponding to E1 vs. E2 classes. Bottom: Coverage across all individual enhancers. **h**. Evolutionary conservation of enhancers separated by enhancer class, as measured by mean phastcon score (probability of each nucleotide belonging to a conserved element) and mean phyloP score (-log(p-value) under a null hypothesis of neutral evolution) across each element. *P*-value from KS test.

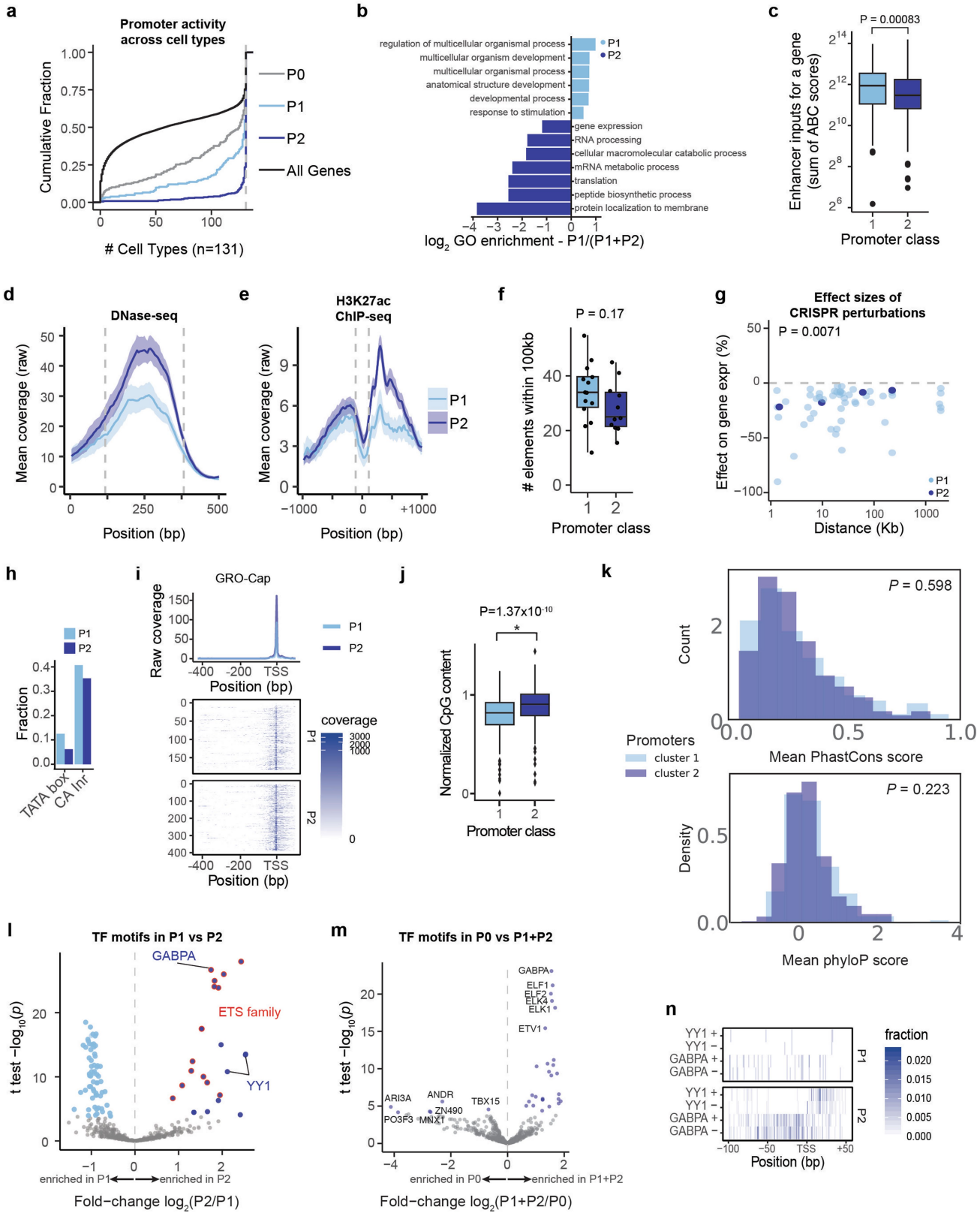

Extended Data Fig. 7 | See next page for caption.

Extended Data Fig. 7 | Properties of promoter classes. a. Cumulative density plot showing the cell-type specificity of promoter chromatin activity (of promoters selected for ExP STARR-seq). X-axis: # of biosamples (cell types or tissues) other than K562 in which the promoter is active. Active = Top 50% of promoters by activity (geometric mean of H3K27ac and DHS signals, as used in the ABC model). All genes = all genes in the genome. **b**. Gene ontology $\log_2$-enrichment for P1 promoters using P1 and P2 promoters as a background set. **c**. Predicted enhancer inputs for each gene (sum of ABC scores for all candidate enhancers within 5 Mb of the TSS, excluding the promoter of the gene itself) for genes in the genome corresponding to P1 versus P2 promoters. $P = 0.00083$, Mann-Whitney U test. Boxes are median and interquartile range, whiskers are +/− 1.5*IQR. **d**. DNase-seq signal in K562 cells at P1 and P2 promoters in the genome, aligned by boundaries of the 264-bp ExP STARR-seq promoter sequence (dotted gray lines, see Methods). **e**. H3K27ac ChIP-seq signal in K562 cells at P1 and P2 promoters in the genome, aligned by boundaries of the 264-bp ExP STARR-seq promoter sequence (dotted grey lines, see Methods). **f**. Number of nearby accessible elements (within 100 Kb of the gene promoter, considering top 150,000 DNase peaks in K562 cells as used in the ABC model[22]) for the 14 genes corresponding to P1 promoters and 11 genes corresponding to P2 promoters with comprehensive CRISPR tiling data. $P = 0.17$, Mann-Whitney U test. Boxes are median and interquartile range, whiskers are +/− 1.5*IQR. **g.** % Effect of CRISPRi perturbations to genomic regulatory elements on genes corresponding to P1 vs. P2 promoters. $P = 0.0071$, *t*-test. **h**. Fraction of promoter sequences containing TATA or CA initiator core promoter motifs. **i**. GRO-Cap coverage of genomic promoters aligned by TSS. Top: Mean coverage of genomic promoters corresponding to P1 vs. P2 classes. Bottom: Coverage across all individual promoters. **j**. Normalized CpG-content of P1 and P2 promoter sequences (n = 800), calculated as the ratio of observed to expected CpG = (CpG fraction) / ((GC content)^2 / 2). Boxes are median and interquartile range, whiskers are +/− 1.5*IQR, $P = 1.37*10^{-10}$, *t*-test. **k**. Evolutionary conservation of promoters separated by promoter class, as measured by mean phastcon score (probability of each nucleotide belonging to a conserved element) and mean phyloP score (-log(p-value) under a null hypothesis of neutral evolution) across each element. *P*-value from KS test. **l**. Volcano plot comparing frequency of transcription factor motifs in P2 versus P1 promoter sequences (see Supplementary Table 7). X-axis: ratio of average motif counts in P2 versus P1 promoter sequences. Light blue and dark blue dots: Motifs significantly more frequent in P1 or P2 promoter sequences, respectively. Red outline: significant motifs for ETS family TFs. **m**. Volcano plot comparing frequency of transcription factor motifs in P2 and P1 versus P0 promoter sequences (see Supplementary Table 7). X-axis: ratio of average motif counts in P2 and P1 versus P0 promoter sequences. Dark blue dots: Motifs significantly more frequent in P2 and P1 vs. P0 promoter sequences. **n**. Fraction of P2 promoter sequences with YY1 and GABPA binding motifs by nucleotide position, aligned by TSS and separated by strand (see Methods).

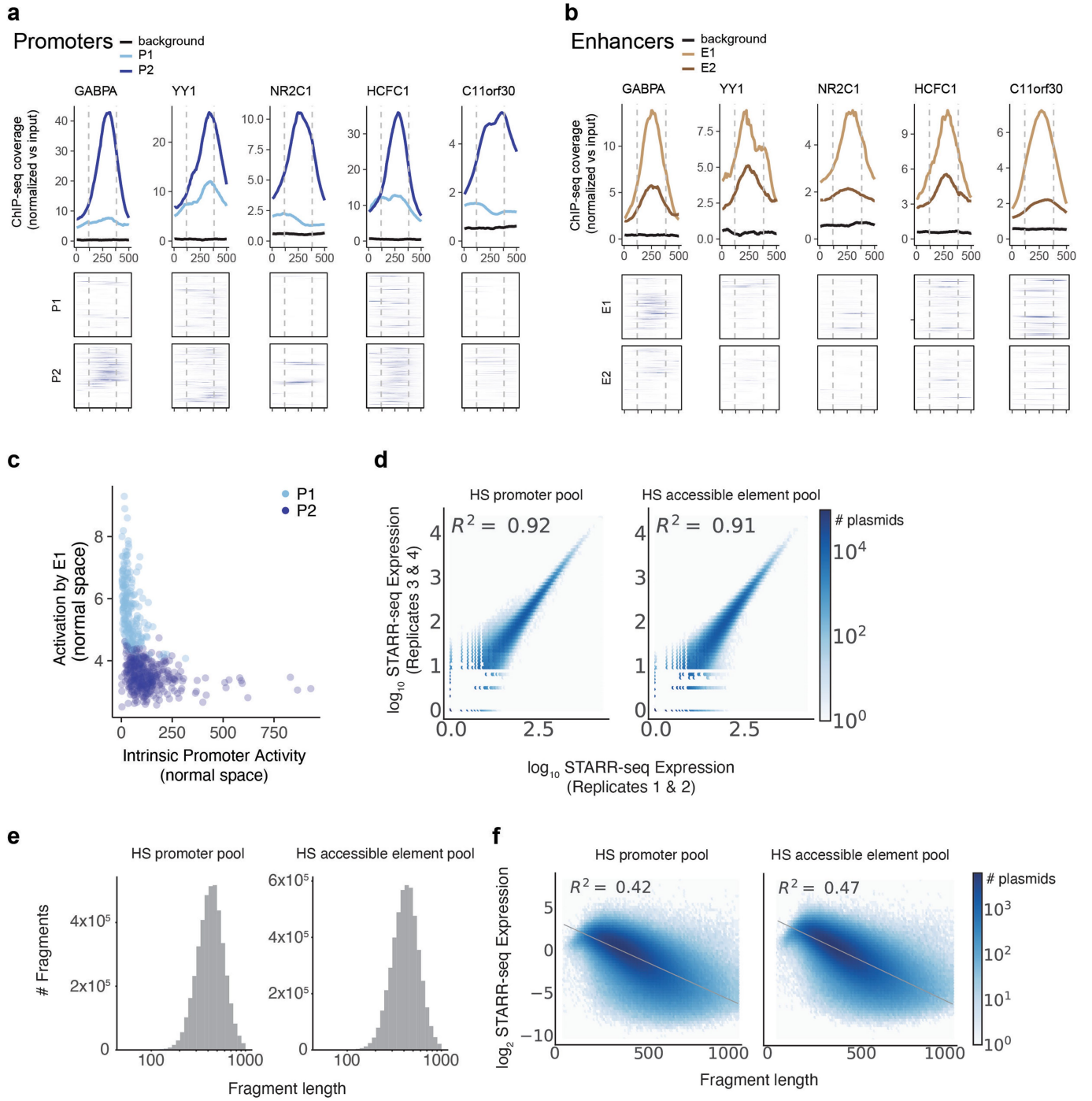

Extended Data Fig. 8 | Transcription factors enriched at promoters and enhancers and hybrid-selection STARR-seq in K562 cells. a. ChIP-seq signal for 5 transcription factors in K562 cells at P1 and P2 promoters in the genome, aligned by boundaries of the 264-bp ExP STARR-seq promoter sequence (see Methods). Top: average ChIP-seq signal normalized to input. Bottom: signal at individual genomic promoters. Black line: average for random genomic control sequences. **b**. ChIP-seq signal at E1 and E2 enhancers in the genome. Black line: average for random genomic control sequences. **c**. Correlation between intrinsic promoter activity and responsiveness of promoters to E1 enhancers (average activation by E1 sequences, expressions vs. random genomic controls). Each point is one promoter. Same as Fig. 5b, but in normal scale instead of $\log_2$ scale. **d**. Correlation of HS-STARR-seq expression between biological replicate experiments for promoter and accessible element pools, calculated for individual elements with unique plasmid barcodes. Axes represent the average STARR-seq expression (RNA/DNA, $\log_{10}$ scale) of two biological replicates. Density: number of plasmids. **e**. Fragment length distribution in HS-STARR-seq in promoter and accessible element pools, of fragments with at least 25 DNA counts. **f**. STARR-seq expression (y-axis) and fragment length (x-axis) relationship in HS-STARR-seq. Density: number of plasmids.

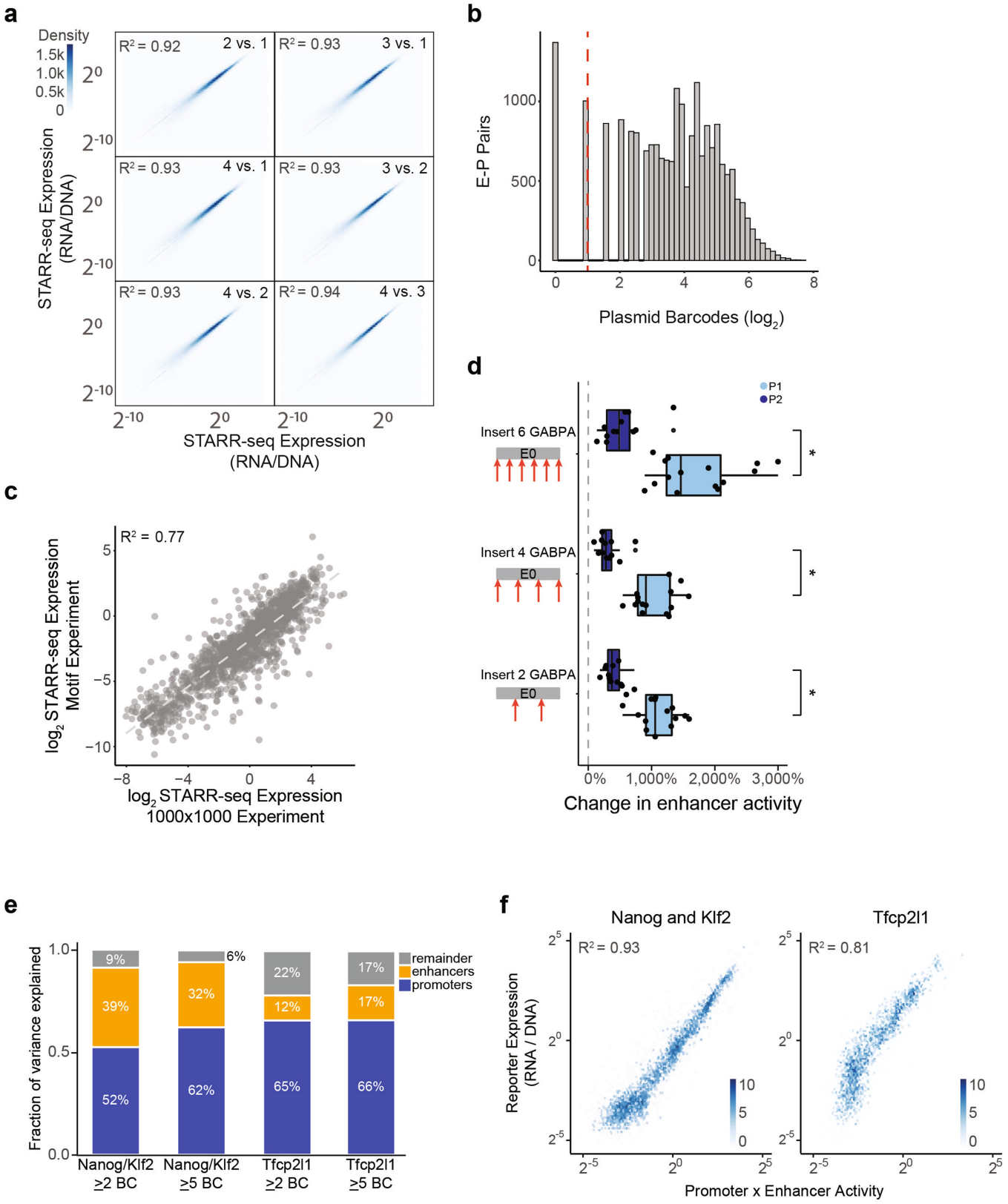

Extended Data Fig. 9 | See next page for caption.

Extended Data Fig. 9 | Motif insertion and scramble ExP STARR-seq in K562 cells and generalizability of compatibility rules. a. Correlation of ExP STARR-seq expression between biological replicate experiments, calculated for individual enhancer-promoter pairs with unique plasmid barcodes. Axes represent the average STARR-seq expression (RNA/DNA) of individual biological replicates. Density: number of enhancer-promoter plasmids. **b**. Distribution of plasmid barcodes per enhancer-promoter pair. Red dotted-line: threshold of two plasmid barcodes. **c**. STARR-seq expression in smaller-scale validation experiment (y-axis) vs. expression in the original ExP STARR-seq dataset (x-axis) for each enhancer-promoter pair included in both experiments. Dotted gray line: line of best fit from linear regression in log2 space. **d**. Change in enhancer activity with P1 or P2 promoters (edited enhancer activity compared with unedited enhancer activity with a promoter) after inserting 2, 4, or 6 GABPA motifs into 1 E0 enhancer sequence. Each point represents one enhancer-promoter pair measured over 4 biological replicates. $^{*}P < 0.0001$, two-tailed *t*-test. Boxes are median and interquartile range, whiskers are +/− 1.5*IQR. **e**. Fraction of variance explained by intrinsic promoter activity and enhancer activity with respect to log2 reporter expression (reporter assay score) from Martinez-Ara *et al*. 2021[39]. Left bars: experiment including promoters and enhancers from the *Nanog* and *Klf2* loci. Right bars: experiment including promoters and enhancers from the *Tfcp2l1* locus. For each experiment, values are shown for pairs with 2 or more, or 5 or more plasmid barcodes. Enhancer and promoter activities explain more of the variance when considering enhancer-promoter pairs with at least 5 vs. at least 2 barcodes. Bar plots show sequential sum of squares (Type-I ANOVA) for promoters, then enhancers. **f**. Correlation of reporter assay expression with the product of intrinsic promoter and enhancer activities from two experiments from Martinez-Ara *et al*., 2021[39]. Density color scale: number enhancer-promoter pairs.

a

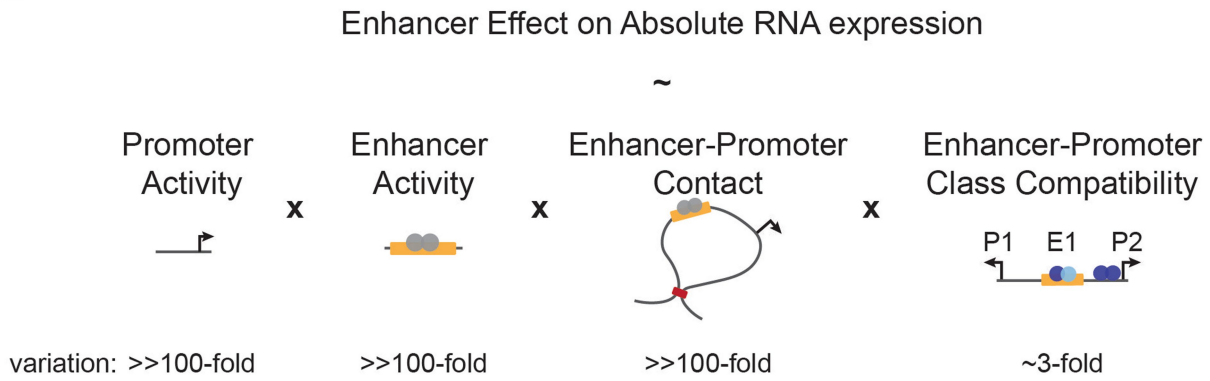

Extended Data Fig. 10 | Model of the effect of an enhancer on RNA expression. a. Simple rules of enhancer and promoter compatibility. The effects of enhancers on nearby genes in the human genome are controlled by the quantitative tuning of intrinsic promoter activity, intrinsic enhancer activity, enhancer-promoter 3D contact, and enhancer-promoter class compatibility.

nature portfolio

Corresponding author(s): Jesse Engreitz

Last updated by author(s): Apr 29, 2022

Reporting Summary

Nature Portfolio wishes to improve the reproducibility of the work that we publish. This form provides structure for consistency and transparency in reporting. For further information on Nature Portfolio policies, see our Editorial Policies and the Editorial Policy Checklist.

Statistics

For all statistical analyses, confirm that the following items are present in the figure legend, table legend, main text, or Methods section.

n/a	Confirmed
☐	☒ The exact sample size (*n*) for each experimental group/condition, given as a discrete number and unit of measurement
☐	☒ A statement on whether measurements were taken from distinct samples or whether the same sample was measured repeatedly
☐	☒ The statistical test(s) used AND whether they are one- or two-sided *Only common tests should be described solely by name; describe more complex techniques in the Methods section.*
☒	☐ A description of all covariates tested
☐	☒ A description of any assumptions or corrections, such as tests of normality and adjustment for multiple comparisons
☐	☒ A full description of the statistical parameters including central tendency (e.g. means) or other basic estimates (e.g. regression coefficient) AND variation (e.g. standard deviation) or associated estimates of uncertainty (e.g. confidence intervals)
☐	☒ For null hypothesis testing, the test statistic (e.g. *F*, *t*, *r*) with confidence intervals, effect sizes, degrees of freedom and *P* value noted *Give P values as exact values whenever suitable.*
☒	☐ For Bayesian analysis, information on the choice of priors and Markov chain Monte Carlo settings
☒	☐ For hierarchical and complex designs, identification of the appropriate level for tests and full reporting of outcomes
☐	☒ Estimates of effect sizes (e.g. Cohen's *d*, Pearson's *r*), indicating how they were calculated

Our web collection on statistics for biologists contains articles on many of the points above.

Software and code

Policy information about availability of computer code

Data collection	N/A
Data analysis	Data was processed using bowtie2 2.3.4.1, R 4.0.2, python 3.6.3, numpy 1.17.4, scipy 1.5.4, pandas 1.1.5, matplotlib 3.3.4, seaborn 0.11.1, sklearn 0.21.3, ncls 0.0.51, statsmodels 0.12.2. Custom code for processing STARR-seq is available at https://github.com/broadinstitute/ExP-model-fit (https://doi.org/10.5281/zenodo.6514733).

For manuscripts utilizing custom algorithms or software that are central to the research but not yet described in published literature, software must be made available to editors and reviewers. We strongly encourage code deposition in a community repository (e.g. GitHub). See the Nature Portfolio guidelines for submitting code & software for further information.

Data

Policy information about availability of data

All manuscripts must include a data availability statement. This statement should provide the following information, where applicable:

- Accession codes, unique identifiers, or web links for publicly available datasets
- A description of any restrictions on data availability
- For clinical datasets or third party data, please ensure that the statement adheres to our policy

Raw and processed data for ExP STARR-seq, motif ExP STARR-seq, HS STARR-seq, and K562 PRO-seq can be found in NCBI GEO under accession number GSE184426. Luciferase data can be found in Supplementary Table S3. Datasets used from the ENCODE Project are listed in Table S9 and are available at https://www.encodeproject.org.

Field-specific reporting

Please select the one below that is the best fit for your research. If you are not sure, read the appropriate sections before making your selection.

☒ Life sciences ☐ Behavioural & social sciences ☐ Ecological, evolutionary & environmental sciences

For a reference copy of the document with all sections, see nature.com/documents/nr-reporting-summary-flat.pdf

Life sciences study design

All studies must disclose on these points even when the disclosure is negative.

Sample size	No statistical methods were used to predetermine sample size. We designed our experiments to maintain a theoretical 100x coverage of each enhancer-promoter pair, and conducted studies in at least biological replicates to ensure reproducibility. The high correlation between biological replicates indicates that these choices were justified.
Data exclusions	No data were excluded from the study.
Replication	STARR-seq and luciferase assay experiments were performed in at least 3 biological replicates and were found to be reproducible. All data are provided in the manuscript.
Randomization	Randomization was not applicable. No case-control study designs were used in this study. All sequences were studied in parallel in the same experiments.
Blinding	No blinding was conducted in this study. The same data filters were applied to all of the thousands of sequences studied here without

Reporting for specific materials, systems and methods

We require information from authors about some types of materials, experimental systems and methods used in many studies. Here, indicate whether each material, system or method listed is relevant to your study. If you are not sure if a list item applies to your research, read the appropriate section before selecting a response.

Materials & experimental systems

n/a	Involved in the study
☒	☐ Antibodies
☐	☒ Eukaryotic cell lines
☒	☐ Palaeontology and archaeology
☒	☐ Animals and other organisms
☒	☐ Human research participants
☒	☐ Clinical data
☒	☐ Dual use research of concern

Methods

n/a	Involved in the study
☒	☐ ChIP-seq
☒	☐ Flow cytometry
☒	☐ MRI-based neuroimaging

Eukaryotic cell lines

Policy information about cell lines

Cell line source(s)	K562 (chronic myelogenous leukemia, ATCC CCL-243)
Authentication	Cell lines were authenticated through RNA-seq and ATAC-seq, followed by comparison to previously published datasets
Mycoplasma contamination	Confirmed negative
Commonly misidentified lines (See ICLAC register)	None